AIP | The Journal of Chemical Physics

Calculating time-resolved differential absorbance spectra for ultrafast pump-probe experiments with surface hopping trajectories

Andrew S. Petit and Joseph E. Subotnik

Citation: The Journal of Chemical Physics **141**, 154108 (2014); doi: 10.1063/1.4897258
View online: http://dx.doi.org/10.1063/1.4897258
View Table of Contents: http://scitation.aip.org/content/aip/journal/jcp/141/15?ver=pdfcov
Published by the AIP Publishing

Articles you may be interested in

Investigation of electronically excited indole relaxation dynamics via photoionization and fragmentation pump-probe spectroscopy
J. Chem. Phys. **141**, 044314 (2014); 10.1063/1.4890875

Vibrational energy relaxation of benzene dimer and trimer in the CH stretching region studied by picosecond time-resolved IR-UV pump-probe spectroscopy
J. Chem. Phys. **136**, 044304 (2012); 10.1063/1.3676658

On the calculation of rotational anisotropy decay, as measured by ultrafast polarization-resolved vibrational pump-probe experiments
J. Chem. Phys. **132**, 174505 (2010); 10.1063/1.3409561

Ultrafast nonradiative dynamics in electronically excited hexafluorobenzene by femtosecond time-resolved mass spectrometry
J. Chem. Phys. **128**, 164314 (2008); 10.1063/1.2907859

Picosecond IR-UV pump-probe spectroscopic study on the intramolecular vibrational energy redistribution of N H 2 and CH stretching vibrations of jet-cooled aniline
J. Chem. Phys. **123**, 124316 (2005); 10.1063/1.2039087



This article is copyrighted as indicated in the article. Reuse of AIP content is subject to the terms at: http://scitation.aip.org/termsconditions. Downloaded to IP: 74.109.53.69 On: Mon, 27 Oct 2014 11:47:44

Calculating time-resolved differential absorbance spectra for ultrafast pump-probe experiments with surface hopping trajectories

Andrew S. Petit and Joseph E. Subotnik
Department of Chemistry, University of Pennsylvania, 231 S. 34th Street, Philadelphia, Pennsylvania 19104, USA

(Received 17 July 2014; accepted 24 September 2014; published online 20 October 2014)

We report a surface hopping approach for modeling the full time- and frequency-resolved differential absorbance spectra (beyond the inhomogenous limit) obtained in ultrafast pump-probe experiments. In our approach, we combine dynamical information obtained from ensembles of classical trajectories propagated on the ground and on the excited potential energy surfaces to directly calculate optical response functions and hence spectral lineshapes. We demonstrate that our method is exact for the model problem of two shifted harmonic potentials with identical harmonic frequencies in the absence of electronic relaxation. We then consider a model three state system with electronic relaxation and show that our method is able to capture the effects of nonadiabatic excited state dynamics on the time-dependent differential absorbance spectra. Furthermore, by comparing our spectra against those spectra calculated with either an (1) inhomogenous expression, (2) ground-state Kubo theory, or (3) excited-state Kubo theory, we show that including dynamical information from both the ground and excited potential energy surfaces significantly improves the reliability of the semiclassical approximations. As such, our surface hopping method should find immediate use in modeling the time-dependent differential abosrbance spectra of ultrafast pump-probe experiments. © *2014 AIP Publishing LLC*. [http://dx.doi.org/10.1063/1.4897258]

I. INTRODUCTION

With the advent of femtosecond laser pulses, nonlinear spectroscopy has become a powerful experimental tool for probing chemical reactions, photochemistry, energy transfer, and nonadiabatic dynamics in real time.[1–13] The interpretation and theoretical modeling of these experiments often begins with the application of perturbation theory to the field-matter interactions, leading to an expansion of the optical response of the molecular system in orders of the applied field,[7,8,14–25] although nonperturbative approaches have been reported.[16,26,27] In particular, outside of anisotropic systems, nonlinear spectroscopy is dominated by third-order processes in which the system experiences three interactions with the applied electromagnetic fields.[7,8]

Pump-probe experiments represent an important subset of nonlinear spectroscopy. In these experiments, the system is first subjected to a pump pulse that creates a wave packet on an excited potential energy surface (PES). After a delay time (t_0), during which the wave packet evolves on the excited PES, the wave packet is interrogated by a probe pulse. By varying the time delay between the femtosecond laser pulses, the dynamics of the wave packet can be monitored in real time.[7,8] In some pump-probe experiments, the experimental signal can be well approximated by averaging the vertical energy gap over an ensemble of trajectories, with the contribution from each trajectory weighted by the square of the transition dipole moment matrix element.[28–32] In the language of Kubo theory,[33] this represents the so-called inhomogeneous part of the spectrum, which will be valid when the energy gap fluctuates slowly relative to nuclear relaxation. This approximation should apply, for example, in the case of time-resolved photoelectron spectroscopy, where a probe pulse ionizes the molecule and the distribution of kinetic energies of the ejected electron are observed as a function of the delay time.[34–36] More generally, without the electronic dissipation present in a photoemission experiment, the output of a pump-probe experiment can be related to a coherence created by the probe pulse that is dependent on the time-delay between the pulses. This coherence is associated with a time-dependent polarization in the sample that radiates an optical signal which can be measured with both time- and frequency-resolution.[7,14,15,37,38]

In this study, we will focus on the standard time-dependent differential absorbance spectra associated with ultrafast pump-probe experiments, where all states are electronically bound. To be more concrete, consider a two-electronic state system described by the Hamiltonian $\hat{H} = |g\rangle\hat{H}_g\langle g| + |e\rangle\hat{H}_e\langle e|$, where $\hat{H}_g$ and $\hat{H}_e$ are the nuclear Hamiltonians associated with the ground and excited electronic states, respectively. These electronic states are coupled through the transition dipole moment operator $\hat{\mu} = |e\rangle\mu_{eg}\langle g| + |g\rangle\mu_{ge}\langle e|$, which we will assume to be position independent following the Condon approximation. We work in the limit of ultrashort pump and probe pulses so that each is approximated as a δ-function in time, with the pump and probe pulses incident at $t = 0$ and $t = t_0$, respectively. Specifically, the pump and probe pulses have the forms $E_{\text{pump}}(t) = E_{\text{pump}}\delta(t)$ and $E_{\text{probe}}(t) = E_{\text{probe}}\delta(t - t_0)$, where we have assumed that the pulses have parallel polarization. Finally, we will neglect the vectorial nature of the light-matter interaction throughout this work.

In the limit of ultrashort pump and probe pulses, Mathies and co-workers demonstrated that the nonlinear

 © 2014 AIP Publishing LLC

This article is copyrighted as indicated in the article. Reuse of AIP content is subject to the terms at: http://scitation.aip.org/termsconditions. Downloaded to IP: 74.109.53.69 On: Mon, 27 Oct 2014 11:47:44

optical response function relevant for calculating time-dependent differential absorbance spectra has the form of a dipole-dipole correlation function with a non-stationary initial state.[7,14,15,38,39] Specifically, for the two-electronic state system introduced above, the dipole-dipole correlation function associated with stimulated emission, which is the dominant contribution to the non-linear signal when the pump pulse is ultrashort, is given by

$$C_{\mu\mu}(\tau, t_0) = \langle \Psi^{(1)}(t_0)| e^{i\hat{H}_e \tau/\hbar} \hat{\mu}_{eg} e^{-i\hat{H}_g \tau/\hbar} \hat{\mu}_{ge} |\Psi^{(1)}(t_0)\rangle = \langle \Psi^{(1)}(t_0)| \langle e|\hat{\mu}(\tau)\hat{\mu}|e\rangle |\Psi^{(1)}(t_0)\rangle, \quad (1)$$

where $\tau = t - t_0$. The non-stationary initial state in Eq. (1) is

$$|\Psi^{(1)}(t_0)\rangle = \frac{i E_{\text{pump}}}{\hbar} e^{-i\hat{H}_e t_0} \hat{\mu}_{eg} |\Psi^{(0)}(0)\rangle, \quad (2)$$

where $|\Psi^{(0)}(0)\rangle$ is the initial vibrational wave function on the ground PES. Equation (2) physically represents a wave packet that was prepared on the excited PES by the pump pulse and subsequently evolved on the excited PES throughout the delay time between the pulses. Within the Condon approximation, $C_{\mu\mu}(\tau, t_0)$ is directly proportional to an electronic coherence between the ground and excited states, $\sigma_{eg}(\tau, t_0)$, created by the probe pulse, so that $C_{\mu\mu}(\tau, t_0) = |\mu_{eg}|^2 \sigma_{eg}(\tau, t_0)$. This electronic coherence evolves in time according to the time-dependent overlap between one wave packet transferred to the ground PES by the probe pulse, $e^{-i\hat{H}_g \tau/\hbar} \hat{\mu}_{ge} |\Psi^{(1)}(t_0)\rangle$, and a second wave packet that continues to evolve on the excited PES, $\hat{\mu}_{ge} e^{-i\hat{H}_e \tau/\hbar} |\Psi^{(1)}(t_0)\rangle$. It is worth noting that Eqs. (1) and (2) only describe the differential absorbance of the probe pulse, i.e., the third-order, nonlinear signal that is generated by the combined effects of the pump and probe pulses – without any contribution from the linear absorption of the probe pulse alone.[14,15]

Several semiclassical approximations to the quantum dynamics present in expressions like Eqs. (1) and (2) are possible.[8,20–22,27–29,33,40–54] For example, according to the formalism of Kubo,[33,45] the electronic coherence of Eq. (1) can be determined using an ensemble of classical trajectories evolved on the ground PES, $\{\vec{x}^{(g)}, \vec{p}^{(g)}\}$,

$$\left\langle \sigma_{eg}^{(g)}(\tau, t_0) \right\rangle_{t_0} = \left\langle \exp\left[-\frac{i}{\hbar} \int_0^\tau d\tau' (H_e(\vec{x}^{(g)}(\tau', t_0), \vec{p}^{(g)}(\tau', t_0)) - H_g(\vec{x}^{(g)}(\tau', t_0), \vec{p}^{(g)}(\tau', t_0))) \right\rangle_{t_0} \sigma_{eg}(t_0). \quad (3)$$

Here, $\sigma_{eg}(t_0) = 1/2$ is the initial value of the electronic coherence created by the probe pulse and $\langle \ldots \rangle_{t_0}$ denotes averaging over an ensemble of classical trajectories that have been propagated on the excited surface throughout the delay time to approximate Eq. (2). Physically, the ground-state Kubo approach relates the time-dependence of the electronic coherence to the distribution of electronic energy gaps sampled by a nuclear wave packet evolving on the ground PES with, generally, non-equilibrium initial conditions determined by the delay time. Alternatively, the trajectories can also be propagated on the excited PES during the evolution of the electronic coherence, yielding the excited-state Kubo expression:

$$\left\langle \sigma_{eg}^{(e)}(\tau, t_0) \right\rangle_{t_0} = \left\langle \exp\left[-\frac{i}{\hbar} \int_0^\tau (H_e(\vec{x}^{(e)}(\tau', t_0), \vec{p}^{(e)}(\tau', t_0)) - H_g(\vec{x}^{(e)}(\tau', t_0), \vec{p}^{(e)}(\tau', t_0))) d\tau' \right\rangle_{t_0} \sigma_{eg}(t_0). \quad (4)$$

Finally, following the semiclassical analysis of Kapral and Martens that leads to the Quantum-Classical Liouville Equation, one finds a third option, namely, that classical trajectories should be propagated on the mean PES,[22,48,50,55–57] so that

$$\left\langle \sigma_{eg}^{(\frac{g+e}{2})}(\tau, t_0) \right\rangle_{t_0} = \left\langle \exp\left[-\frac{i}{\hbar} \int_0^\tau (H_e(\vec{x}^{(\frac{g+e}{2})}(\tau', t_0), \vec{p}^{(\frac{g+e}{2})}(\tau', t_0)) - H_g(\vec{x}^{(\frac{g+e}{2})}(\tau', t_0), \vec{p}^{(\frac{g+e}{2})}(\tau', t_0))) d\tau' \right\rangle_{t_0} \sigma_{eg}(t_0). \quad (5)$$

Equations (3)–(5) represent three similar (but distinct) formalisms for calculating spectra. In a recent study,[58] we developed a fourth semiclassical approximation to the calculation of electronic coherences:

$$C_{\mu\mu}^{(\text{SC})}(\tau, t_0) = |\mu_{eg}|^4 \frac{\sqrt{\left\langle \sigma_{eg}^{(g)}(\tau, t_0) \right\rangle_{t_0} \left\langle \sigma_{eg}^{(e)}(\tau, t_0) \right\rangle_{t_0}}}{\sigma_{eg}(t_0)}, \quad (6)$$

where the transition dipole moment is raised to the fourth power to reflect the combined effects of the pump and probe pulses. By taking a geometric average of $\langle \sigma_{eg}^{(g)}(\tau, t_0) \rangle_{t_0}$ and $\langle \sigma_{eg}^{(e)}(\tau, t_0) \rangle_{t_0}$, Eq. (6) includes dynamical information obtained on both PESs in a balanced way which results in greater accuracy than either Kubo approach alone. As shown in Appendix A, Eq. (6) is exact for the model problem of two shifted harmonic potentials with identical harmonic frequencies. Moreover, as shown in Appendix B of our previous study on linear absorption spectra,[58] $\sqrt{\langle \sigma_{eg}^{(g)}(\tau, t_0) \rangle_{t_0} \langle \sigma_{eg}^{(e)}(\tau, t_0) \rangle_{t_0}} / \sigma_{eg}(t_0)$ evolves in a manner consistent with the Quantum-Classical Liouville Equation for short times.[59] A numerical comparison between spectra calculated using Eq. (6) and the results of Eqs. (3)–(5) is provided below for two shifted harmonic potentials with different harmonic frequencies.

Our major goal in this work is to extend Eq. (6) to systems in which nonadiabatic excited-state dynamics are important. In doing so, we will use swarms of mixed quantum-classical trajectories propagated using Tully's fewest switches surface hopping (FSSH) algorithm,[60,61] which we believe is an excellent compromise between accuracy and computational efficiency. We are not the first to develop semiclassical descriptions of pump-probe spectroscopy that include the effects of nonadiabatic wave packet dynamics.[19,27,29–32,62] Indeed, surface hopping approaches have previously been used to model the inhomogeneous component of pump-probe signals associated with time-resolved photoelectron

This article is copyrighted as indicated in the article. Reuse of AIP content is subject to the terms at: http://scitation.aip.org/termsconditions. Downloaded to IP: 74.109.53.69 On: Mon, 27 Oct 2014 11:47:44

spectroscopy and time-resolved absorption.[29,31,32,63] FSSH has also recently been used to introduce electronic relaxation during the evolution of electronic populations as part of a larger calculation of two-dimensional electronic spectra.[23] However, the historical absence of a well-defined FSSH density matrix has prevented the use of FSSH to calculate quantities directly related to electronic coherences, such as dipole-dipole correlation functions and hence time-dependent differential absorbance spectra beyond the inhomogeneous limit. The complication in doing so arose because each trajectory carries both an electronic wave function and an active adiabatic surface so that some electronic information appears to be effectively double counted. Several researchers have attempted to use either the electronic wave function or the active adiabatic surface information to build up an approximate FSSH density matrix, although none of these approaches were fully satisfactory.[23,64–68]

In a series of recent papers, our group has established the mixed quantum-classical nuclear-electronic density matrix consistent with a swarm of FSSH trajectories.[69,70] Using this FSSH density matrix, we recently demonstrated that dipole-dipole correlation functions associated with linear absorption can be directly calculated from ensembles of FSSH trajectories propagated on the ground and excited PESs.[58] In this study, we extend these ideas to model the full time- and frequency-resolved differential absorbance spectra (beyond the inhomogeneous limit) associated with ultrafast pump-probe spectroscopy in systems that exhibit significant nonadiabatic excited state dynamics.

Before concluding this introduction, it is worth emphasizing that the calculation of dipole-dipole correlation functions directly from FSSH trajectories represents a major challenge for two reasons. First, the time-dependence of $C_{\mu\mu}(t)$ reflects details of how wave packets evolving on the ground and excited PESs repeatedly separate and recombine. Nuclear quantum effects associated with wave packet separation and recombination, such as decoherence and recoherence, cannot be fully captured by swarms of non-interacting FSSH trajectories.[69,71] However, as shown in our previous study on the calculation of linear absorption spectra using FSSH, swarms of FSSH trajectories can sometimes provide a reasonable approximation for recoherences associated with the time dependent overlap of nuclear wave packets moving on different surfaces.[58] Moreover, a number of extensions to FSSH have been developed that include approximate effects of decoherence, including our group's AFSSH algorithm.[69,71–77] Second, in principle, the dynamics underlying $C_{\mu\mu}(t)$ must be stable for long enough periods of time for the dipole-dipole correlation function to decay to zero and, as a result, short-time approximations may not suffice. This is particularly relevant for gas phase systems which do not have environmental interactions with which to damp out the long time oscillations of $C_{\mu\mu}(t)$. As such, the gas phase model systems considered in this study represent a stringent test of the limits of our approach. That being said, we will show below that our methodology is based upon a short-time approximation of wave packet coherences. In practice, this implies that FSSH will be most useful for condensed phase spectroscopy. After all, as originally argued by Heller, modeling the spectral line shapes associated with electronic spectroscopy requires dipole-dipole correlation functions to be evaluated over only short times.[40]

II. THEORY

A. The semiclassical calculation of time-dependent differential absorbance spectra in the presence of nonadiabatic dynamics

In this paper, we will focus on systems in which, in the *diabatic representation*, the transition dipole moment is position independent and couples the ground state (state 1) to a single (bright) excited state (state 2). The bright excited state is vibronically coupled to one or more dark excited states but we will assume that no vibronic coupling exists between the ground and excited states. We will work in the limit of ultrashort pump and probe pulses and focus on the time-dependent differential absorbance spectra associated with stimulated emission. Note that extending the approach developed below to excited-state absorption would only require switching the ground state with any additional excited state(s) encountered during the evolution of the electronic coherence.

Turning to the details of our approach, we first develop a semiclassical approximation for the non-stationary initial conditions in Eq. (1), $|\Psi^{(1)}(t_0)\rangle$, in terms of an ensemble of FSSH trajectories. The initial positions and momenta are sampled from the Wigner distribution of the ground vibrational state on the ground PES.[78,79] Note that the use of the appropriate Wigner distribution to initialize the ensemble of trajectories ensures that the semiclassical and quantum nuclear density matrices agree at the start of the calculation; we assume that there is no nuclear-electronic entanglement at $t = 0$. Because the adiabatic, $\{|\Phi_i\rangle\}$, and diabatic, $\{|\Xi_a\rangle\}$, electronic bases are related by a position-dependent unitary transformation, $\mathbf{U}(\vec{x})$, the electronic wave function for the ℓth trajectory can be expressed in either basis as

$$\sum_i c_i^{[\ell]}|\Phi_i\rangle = \sum_{ia} U_{ai}^{[\ell]}(\vec{x}^{\,[\ell]})c_i^{[\ell]}|\Xi_a\rangle = \sum_a b_a^{[\ell]}|\Xi_a\rangle. \quad (7)$$

As we are focusing on stimulated emission, only population excited by the pump pulse at $t = 0$ will contribute. Therefore, all trajectories are initialized on the bright state so that $b_2^{[\ell]}(0) = 1$ and $b_{k\neq 2}^{[\ell]}(0) = 0$ or, in the adiabatic representation, $c_k^{[\ell]}(0) = U_{2k}(\vec{x}^{\,[\ell]}(0))$. The active adiabatic potential for the ℓth trajectory, $\lambda^{[\ell]}(0)$, is stochastically determined based on the adiabatic probability amplitudes $|c_k^{[\ell]}(0)|^2$. The swarm of mixed quantum-classical trajectories are then propagated using FSSH throughout the delay time from $t = 0$ to $t = t_0$.

Second, we turn to how the mixed quantum-classical trajectories are modified by the probe pulse at $t = t_0$, the overall effect of which is to create an electronic coherence between the ground and bright *diabatic states*. Incorporating the effects of the pump pulse is a tricky task because one must modify both the electronic wave functions and active adiabatic surfaces consistently. Nevertheless, we believe that there is only one stable way forward. Because the electronic

This article is copyrighted as indicated in the article. Reuse of AIP content is subject to the terms at: http://scitation.aip.org/termsconditions. Downloaded to IP: 74.109.53.69 On: Mon, 27 Oct 2014 11:47:44

wave functions have phases which can interfere when averaged over a swarm of trajectories, any attempt to estimate the true electronic coherence from the electronic wave function of a single trajectory can result in large errors. By contrast, the active adiabatic surface of each trajectory represents a positive weight for the population density. Therefore, it is much safer to focus on the active adiabatic surfaces, particularly for long times.[70,80,81] As such, at the moment of the probe pulse, our protocol is to preserve $\lambda^{[\ell]}(t_0)$ and reset the adiabatic expansion coefficients so that $c_1^{[\ell]}(t_0) = 1/\sqrt{2}$ and $c_{\lambda^{[\ell]}(t_0)}^{[\ell]}(t_0) = 1/\sqrt{2}$, while all other coefficients are set equal to zero. It is worth noting that although this procedure for initializing the electronic coherence is not unique, it is both the most effective and the most straightforward of the schemes that we studied numerically.

The third step is to evaluate Eq. (4) as a Monte Carlo average over this ensemble of FSSH trajectories. Following Ref. 58, we first define the quantum-classical, nuclear-electronic density matrix consistent with an ensemble of FSSH trajectories, $\mathbf{A}(\vec{x}, \vec{p}, \tau, t_0)$, as

$$A_{jk}(\vec{x}, \vec{p}, \tau, t_0) = \frac{1}{N_{\text{traj}}} \sum_{\ell=1}^{N_{\text{traj}}} \delta(\vec{x} - \vec{x}^{\,[\ell]}(\tau, t_0))\delta(\vec{p} - \vec{p}^{\,[\ell]}(\tau, t_0)) \times \frac{\sigma_{jk}^{[\ell]}(\tau, t_0)}{\sigma_{jj}^{[\ell]}(\tau, t_0) + \sigma_{kk}^{[\ell]}(\tau, t_0)} (\delta_{j\lambda^{[\ell]}(\tau,t_0)} + \delta_{k\lambda^{[\ell]}(\tau,t_0)}), \quad (8)$$

where $\sigma_{jk}^{[\ell]}(t) = c_j^{[\ell]}(t)c_k^{[\ell]*}(t)$ is an element of the electronic density matrix carried by the ℓth trajectory.[58,69,70] Note that $\mathbf{A}(\vec{x}, \vec{p}, \tau, t_0)$ is defined at each geometry in terms of the *adiabatic electronic basis* for that geometry and that only those trajectories moving along the jth or kth adiabats at time t contribute to $A_{jk}(\vec{x}, \vec{p}, \tau, t_0)$. Importantly, the electronic coherence that enters into Eq. (6) is between the ground and bright excited *diabatic states*. Using $\mathbf{U}(\vec{x})$, the FSSH nuclear-electronic density matrix is converted into the diabatic representation via $\mathbf{B}(\vec{x}, \vec{p}, \tau, t_0) = \mathbf{U}(\vec{x})\mathbf{A}(\vec{x}, \vec{p}, \tau, t_0)\mathbf{U}^{\dagger}(\vec{x})$. The electronic coherence between the ground and bright excited diabatic states, $\langle\sigma_{21}^{(\text{diab})}(\tau, t_0)\rangle_{t_0}$, is then calculated using

$$\left\langle\sigma_{21}^{(\text{diab})}(\tau, t_0)\right\rangle_{t_0} = \frac{1}{N_{\text{traj}}} \sum_{\ell=1}^{N_{\text{traj}}} \sum_{jk} U_{2j}(\vec{x}^{\,[\ell]}(\tau, t_0))U_{1k}^{*}(\vec{x}^{\,[\ell]}(\tau, t_0)) \times \frac{\sigma_{jk}^{[\ell]}(\tau, t_0)}{\sigma_{jj}^{[\ell]}(\tau, t_0) + \sigma_{kk}^{[\ell]}(\tau, t_0)} (\delta_{j\lambda^{[\ell]}(\tau,t_0)} + \delta_{k\lambda^{[\ell]}(\tau,t_0)}), \quad (9)$$

where we have implicitly integrated Eq. (8) over all nuclear positions and momenta. Performing this analysis using the ensemble of trajectories described above results in the calculation of $\langle\sigma_{21}^{(\text{diab, e})}(\tau, t_0)\rangle_{t_0}$.

The fourth and final step is to generalize Eq. (6) to account for the presence of nonadiabatic excited state dynamics. In order to do so, we need to develop a second ensemble of mixed quantum-classical trajectories to represent the nuclear wave packet transferred to the ground PES by the probe pulse. This is accomplished by creating a copy of the above ensemble at $t = t_0$ with identical electronic wave functions and nuclear positions and momenta but with $\lambda^{[\ell]}(t_0) = 1$. That is, at the onset of the electronic coherence, the trajectories in this second ensemble are all initialized on the ground PES. This ensemble is propagated using FSSH and $\langle\sigma_{21}^{(\text{diab, g})}(\tau, t_0)\rangle_{t_0}$ is calculated using Eq. (9). The dipole-dipole correlation function is then determined by combining $\langle\sigma_{21}^{(\text{diab, g})}(\tau, t_0)\rangle_{t_0}$ and $\langle\sigma_{21}^{(\text{diab, e})}(\tau, t_0)\rangle_{t_0}$ according to

$$\frac{C_{\mu\mu}^{(\text{diab})}(\tau, t_0)}{\left|\mu_{21}^{(\text{diab})}\right|^4} = \frac{\sqrt{\left\langle\sigma_{21}^{(\text{diab, g})}(\tau, t_0)\right\rangle_{t_0}\left\langle\sigma_{21}^{(\text{diab, e})}(\tau, t_0)\right\rangle_{t_0}}}{\sigma_{21}^{(\text{diab})}(t_0)}, \quad (10)$$

where $\sigma_{21}^{(\text{diab})}(t_0) = 1/2$ is the initial electronic coherence when the pump and probe pulses are coincident and is included in Eq. (10) to ensure proper normalization. Finally, note that a generalization of Eqs. (9) and (10) that approximately accounts for non-Condon effects in the *diabatic* representation is presented in Appendix B.

B. A step-by-step algorithm for the calculation of time-dependent differential absorbance spectra using surface hopping

In order to describe our approach as clearly as possible, we provide here a step-by-step algorithm for calculating time-dependent differential absorbance spectra using ensembles of FSSH trajectories. As in Subsection II A, we will assume that, in the *diabatic representation*, there is a single bright excited state as well as at least one dark excited state. We will label the states such that the ground state is state 1 and the bright diabatic state is state 2.

1. Initialize the nuclear positions and momenta of the mixed quantum-classical trajectories by sampling from the appropriate Wigner distribution on the ground PES (state 1).
2. To simulate the effect of the pump pulse, initialize the electronic wave functions such that all trajectories are initially on the bright diabatic state (state 2). Specifically, the coefficients in the *adiabatic representation* for the ℓth trajectory are given by $c_k^{[\ell]}(0) = U_{2k}(\vec{x}^{[\ell]}(0))$, where $\mathbf{U}(\vec{x})$ is the unitary transformation matrix relating the adiabatic and diabatic electronic bases. The active adiabatic surface for the ℓth trajectory at $t = 0$, $\lambda^{[\ell]}(0)$, is then stochastically determined based on the values of $|c_k^{[\ell]}(0)|^2$.
3. Propagate the ensemble of mixed quantum-classical trajectories using FSSH from $t = 0$ to $t = t_0$, i.e., over the delay time between the pump and probe pulses.
4. To initialize the electronic coherence created by the probe pulse at $t = t_0$, reset the electronic wave functions so that, for the ℓth trajectory with active adiabatic

This article is copyrighted as indicated in the article. Reuse of AIP content is subject to the terms at: http://scitation.aip.org/termsconditions. Downloaded to IP: 74.109.53.69 On: Mon, 27 Oct 2014 11:47:44

surface $\lambda^{[\ell]}(t_0)$, $c_1^{[\ell]}(t_0) = 1/\sqrt{2}$, $c_{\lambda^{[\ell]}(t_0)}^{[\ell]}(t_0) = 1/\sqrt{2}$, and all other coefficients are set equal to zero. Propagate this ensemble using FSSH and at each time step, calculate $\langle \sigma_{21}^{(\text{diab, e})}(\tau, t_0)\rangle_{t_0}$ using Eq. (9).

5. To model the wave packet transferred to the ground adiabatic PES by the probe pulse, create a copy of the ensemble in the previous step at $t = t_0$ with identical electronic wave functions, nuclear positions, and nuclear momenta but with the ground PES as the active adiabatic surface. Propagate this ensemble with FSSH and at each time step, calculate $\langle \sigma_{21}^{(\text{diab, g})}(\tau, t_0)\rangle_{t_0}$ using Eq. (9).
6. Calculate the dipole-dipole correlation function at each time step using Eq. (10). Note that in doing so, the sign of $C_{\mu\mu}(\tau + \delta t, t_0)$ is determined based on which of the roots of Eq. (6) lie closest in the complex plane to $C_{\mu\mu}(\tau, t_0)$.

III. RESULTS AND DISCUSSION

A. Time-dependent differential absorbance spectra in the absence of electronic relaxation: Two shifted harmonic potentials with different harmonic frequencies

We first consider the model problem of two shifted harmonic potentials with different harmonic frequencies defined by the Hamiltonian

$$H_g = \frac{p^2}{2m} + \frac{m\omega_g^2 x^2}{2},$$
$$H_e = \frac{p^2}{2m} + \frac{m\omega_e^2 (x-d)^2}{2} + \epsilon_0, \tag{11}$$

with $\hbar\omega_g = 500\ \text{cm}^{-1}$, $\epsilon_0 = 8000\ \text{cm}^{-1}$, and $m = 1728.26$ a.u. The semiclassical calculations were performed using an ensemble of 80 000 trajectories, with 40 000 trajectories propagated on each surface when Eq. (6) was used. The initial positions and momenta were sampled from the ground state harmonic oscillator Wigner distribution associated with the ground PES and the equations of motion were integrated using the fourth-order Runge Kutta algorithm.[78,79,82] Exact quantum dynamics calculations were performed using the discrete variable representation (DVR) in a sinc-DVR basis with a grid of 4000 evenly spaced points spanning from −12.0 a.u. to 12.0 a.u.[83] For all of the calculations, a time step of $\delta t = 0.05$ fs was used and the electronic coherences were propagated for $\tau_{\text{max}} = 100$ fs. The time-dependent differential absorbance spectra were calculated from $C_{\mu\mu}(\tau, t_0)$ using

$$\alpha(\omega, t_0) \simeq -\frac{8\pi\omega}{c\hbar}\text{Im}\left[\int_0^{\tau_{\text{max}}} e^{i\omega\tau}\,\text{Im}[C_{\mu\mu}(\tau, t_0)]\cos\left(\frac{\pi\tau}{2\tau_{\text{max}}}\right)d\tau\right], \tag{12}$$

where the factor $\cos(\pi\tau/2\tau_{\text{max}})$ was used to reduce the presence of spurious Gibbs oscillations by forcing the integrand to smoothly go to zero at the final time included in the dynamics.[84] Equation (12) was evaluated on a frequency grid containing 3600 evenly spaced points from 2000 cm^{-1} to 14 000 cm^{-1}. Finally, when Eq. (6) was used, the sign of $C_{\mu\mu}(\tau + \delta t, t_0)$ was determined based on which of the roots of Eq. (6) lied closest in the complex plane to $C_{\mu\mu}(\tau, t_0)$.

The time-dependent differential absorbance spectra of the shifted harmonic potentials model with $d = 1.0$ a.u. calculated using Eq. (6) are shown in Figure 1 as the dashed red lines and compared to the results of numerically exact quantum dynamics (solid black lines) and the alternative semiclassical approximations given in Eqs. (3)–(5) (blue dotted lines). Focusing first on the $\omega_e = 0.9\omega_g$ data, the results of semiclassical calculations performed using Eq. (6) are in excellent agreement with the exact spectra and comparable to performing the dynamics on the mean PES, Eq. (5). In contrast, both Kubo approaches, Eqs. (3) and (4), yield qualitatively incorrect spectral line shapes. When the harmonic frequency of the excited PES is reduced to $\omega_e = 0.5\omega_g$, the agreement between the exact spectra and the semiclassical spectra calculated using Eq. (6) is less good. Nevertheless, our approach is able to capture the overall evolution of the spectral line shape with increasing t_0 and is comparable to performing the dynamics on the mean PES. Moreover, the spectra calculated using Eq. (6) are in significantly better agreement with the exact spectra than the ground-state Kubo spectra. That being said, in this case, the excited-state Kubo spectra are in only slightly worse agreement with the exact spectra than the results of Eq. (6).

The effect of increasing the shift between the harmonic potentials to $d = 2.0$ a.u. on the time-dependent differential absorbance spectra and the accuracy of the semiclassical approximations is shown in Figure 2. When $\omega_e = 0.9\omega_g$, Eq. (6) is found to capture the overall evolution of the spectral line shapes with increasing delay time as well as some of the underlying vibrational structure, although some deviations with the exact spectra are present. For this case, performing the dynamics on the mean PES is slightly more successful at capturing the vibrational structure in the spectra. Finally, for this larger shift (d = 2.0 a.u.) between the PESs, the results of both Kubo approaches are in much better agreement with the exact spectra than for the smaller shift ($d = 1.0$ a.u.). (Note that this result is consistent with observations made in our previous study involving linear absorption spectra.[58]) Nevertheless, we emphasize that Eq. (6) still outperforms ground-state Kubo and Eq. (6) is also still in somewhat better agreement with the exact spectra than the excited-state Kubo spectra.[85]

Finally, we turn to the data with $\omega_e = 0.5\omega_g$ and $d = 2.0$ a.u. On the right-hand side of Figure 2, we see that the spectra calculated using Eq. (6) display the same overall spectral line shapes and dependence on t_0 as is found in the exact spectra, although our semiclassical approach cannot fully resolve the vibrational structure. Performing the dynamics on the mean PES results in spectra that are comparable to our approach. The ground-state Kubo spectra display qualitative errors but the excited state Kubo spectra are in only slightly worse agreement with the exact spectra than the results calculated using Eq. (6). A more complete comparison of the performance of the different semiclassical approximations for this model system can be found in Figures S1– S4 in the supplementary material.[85]

This article is copyrighted as indicated in the article. Reuse of AIP content is subject to the terms at: http://scitation.aip.org/termsconditions. Downloaded to IP: 74.109.53.69 On: Mon, 27 Oct 2014 11:47:44

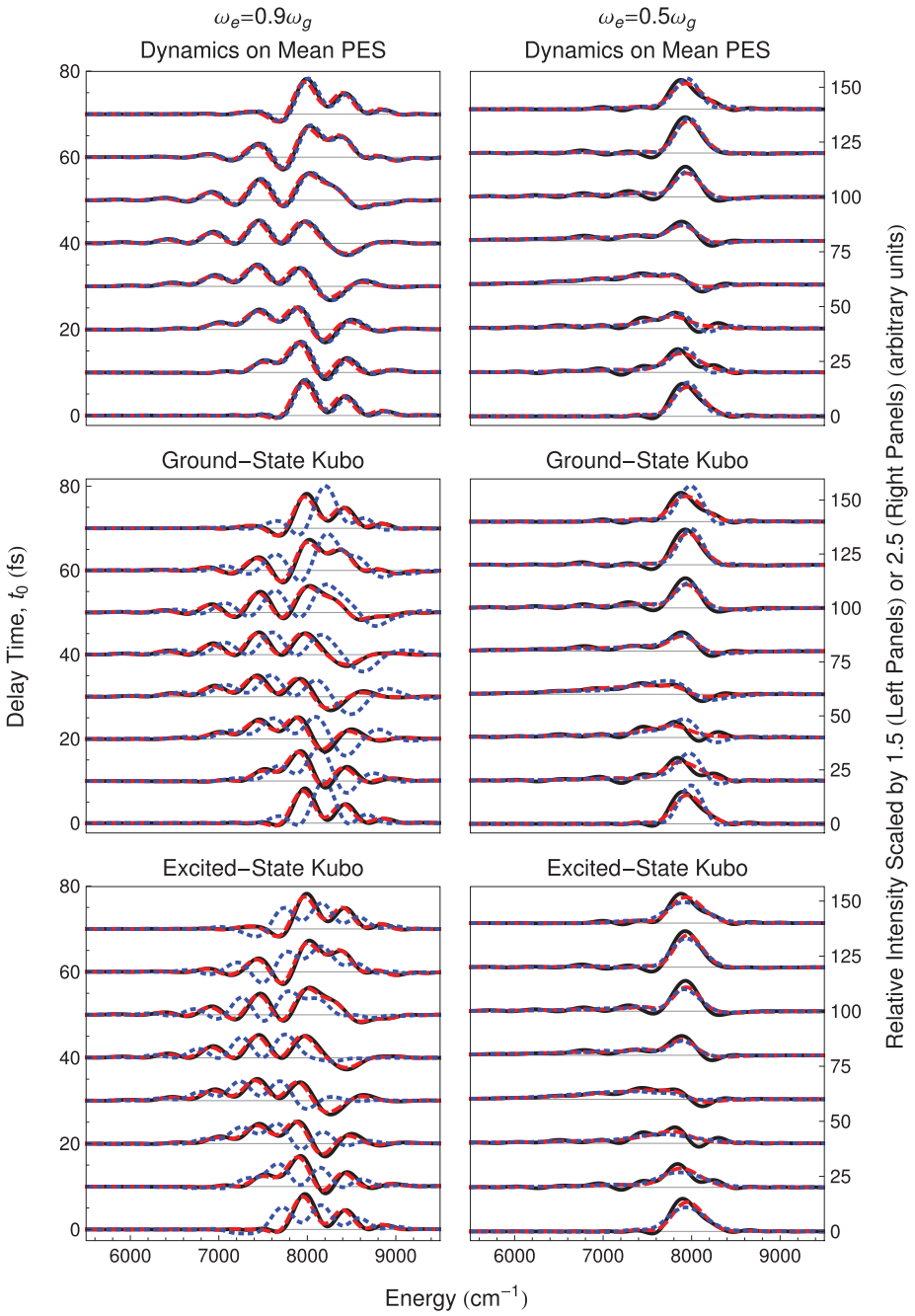


FIG. 1. A comparison between the time-dependent differential absorbance spectra of the shifted harmonic potentials model of Eq. (11) with $d = 1.0$ a.u. and $\omega_e = 0.9\omega_g$ or $\omega_e = 0.5\omega_g$. The spectra are calculated using numerically exact quantum dynamics (solid black lines), semiclassically using Eq. (6) (dashed red lines), and semiclassically using the specified alternative approximation (dotted blue lines).

B. The time-dependent differential absorbance spectra with electronic relaxation: A three state model

We now consider a three state model defined by the *diabatic potentials:*

$$\begin{aligned} V_1(x) &= D_e\,(1-\exp(-\gamma x))^2\,,\\ V_2(x) &= D_e\,(1-\exp(-\gamma(x-d)))^2+\epsilon_0,\\ V_3(x) &= 1.1D_e+\hbar\omega\exp(-4\gamma(x-d_2)), \end{aligned} \tag{13}$$

where $D_e = (\hbar\omega)/(4\alpha_{anh})$, $\gamma = \sqrt{2m\omega\alpha_{anh}/\hbar}$, m is the mass, ω is the harmonic frequency, $d_2 = 2 + d$, and the anharmonicity parameter α_{anh} is defined such that the νth vibrational eigenstate has energy,

$$E_\nu = \hbar\omega\left(\nu+\frac{1}{2}\right)-\alpha_{anh}\hbar\omega\left(\nu+\frac{1}{2}\right)^2. \tag{14}$$

The specific parameters used in this study are $m = 1728.26$ a.u., $\hbar\omega = 500$ cm^{-1}, $\epsilon_0 = 16\,000$ cm^{-1}, and $\alpha_{anh} = 0.01$. Note that with this choice of parameters, the Morse potentials support 49 bound vibrational states. The two excited diabatic states are coupled by a constant diabatic coupling, V_{23}, while no such coupling exists between either excited state and the ground state, $V_{12} = V_{13} = 0$. In the diabatic representation,

This article is copyrighted as indicated in the article. Reuse of AIP content is subject to the terms at: http://scitation.aip.org/termsconditions. Downloaded to IP: 74.109.53.69 On: Mon, 27 Oct 2014 11:47:44

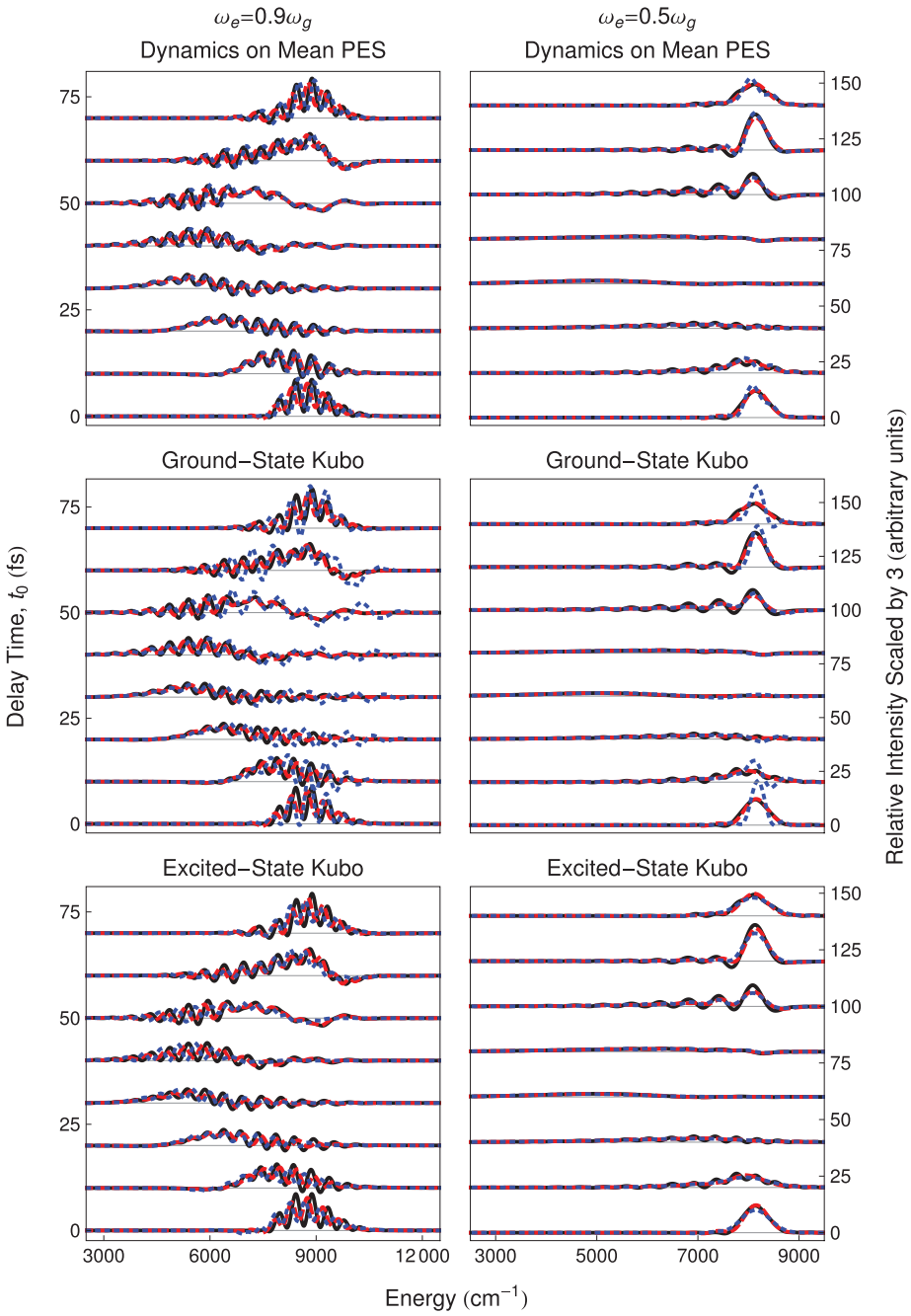


FIG. 2. A comparison between the time-dependent differential absorbance spectra of the shifted harmonic potentials model of Eq. (11) with $d = 2.0$ a.u. and $\omega_e = 0.9\omega_g$ or $\omega_e = 0.5\omega_g$. The spectra are calculated using numerically exact quantum dynamics (solid black lines), semiclassically using Eq. (6) (dashed red lines), and semiclassically using the specified alternative approximation (dotted blue lines).

a position independent transition dipole moment is assumed to exist between states 1 and 2, $\mu_{12}^{(\mathrm{diab})} = 1$ a.u., while the repulsive diabat, $V_3(x)$, is dark. The transition dipole moment operator is readily transformed into the adiabatic representation using $\mathbf{U}(x)$ according to $\hat{\mu}^{(\mathrm{adiab})}(x) = \mathbf{U}^{\dagger}(x)\hat{\mu}^{(\mathrm{diab})}\mathbf{U}(x)$. It is worth noting that $\hat{\mu}^{(\mathrm{adiab})}(x)$ does not satisfy the Condon approximation and couples the ground state to both excited adiabatic states. In this study, the adiabatic transition dipole moments were made continuous by defining the signs of the columns of $\mathbf{U}(x)$ such that $U_{22}(x) > 0$ and $U_{33}(x) > 0$. Plots of representative adiabatic PESs as well as adiabatic transition dipole moments are shown in Figure 3.

In a moment, we will provide the results of applying our semiclassical ansatz (Eqs. (9) and (10)) to this three state model. As a means of evaluating our approximations, we have also considered three other distinct semiclassical approximations that differ from each other and from the approach developed in this study only in how the electronic coherence is described; unless specified otherwise, *all semiclassical approaches used FSSH to propagate the excited populations throughout the delay time*. In the first of these, the ground-state Kubo approach, the trajectories are vertically shifted onto the ground PES at $t = t_0$ and propagated on this surface throughout the calculation of the electronic coherence. In

This article is copyrighted as indicated in the article. Reuse of AIP content is subject to the terms at: http://scitation.aip.org/termsconditions. Downloaded to IP: 74.109.53.69 On: Mon, 27 Oct 2014 11:47:44

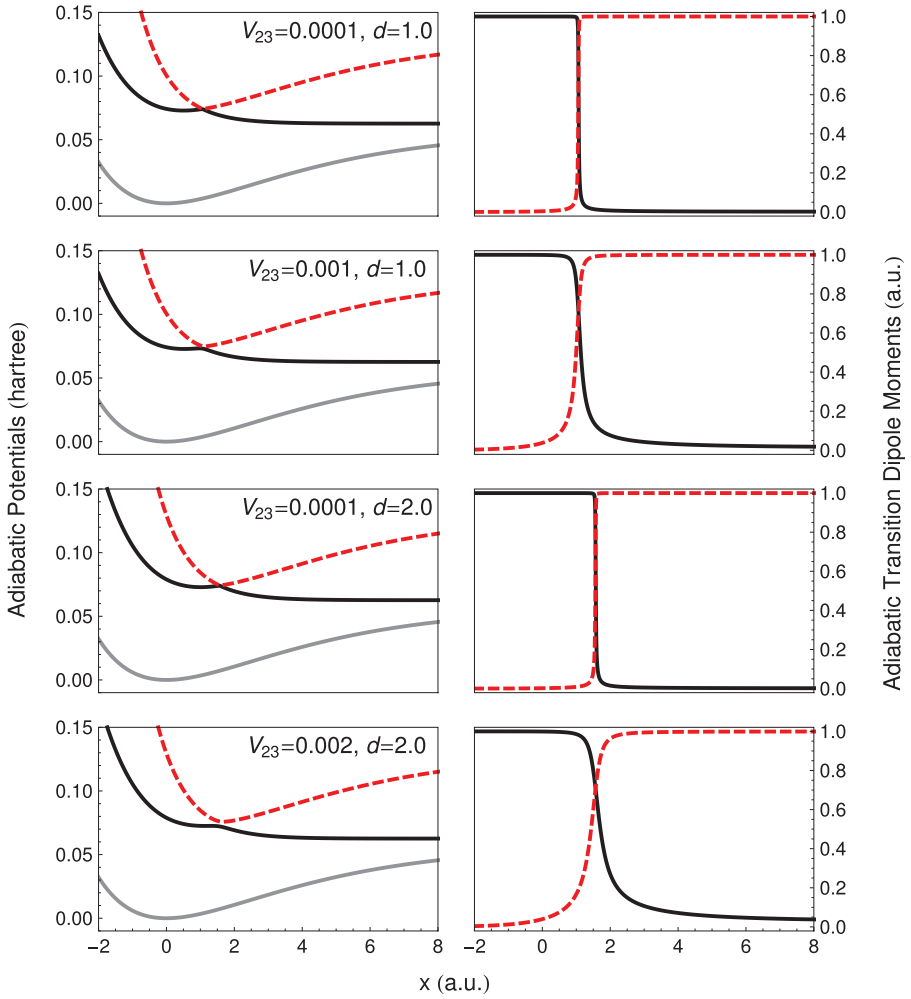


FIG. 3. Adiabatic PESs of the ground (solid gray line), dissociative excited (solid black line), and bound excited (dashed red line) states of the three state model system considered in this study. Also shown are the adiabatic transition dipole moments coupling the ground state to the dissociative excited state (solid black line) and the ground state to the bound excited state (dashed red line).

doing so, it is important to take into account the fact that the adiabatic transition dipole moment ($\hat{\mu}^{(\text{adiab})}(x)$) is position dependent due to $\mathbf{U}(x)$ and $\hat{\mu}^{(\text{adiab})}(x)$ couples the ground state to both excited adiabats. As in our previous study,[58] we define the ground-state Kubo expression for the dipole-dipole correlation function as

$$
\begin{aligned}
&C_{\mu\mu}^{(\text{Kubo, } g)}(\tau, t_0)\frac{N_{\text{traj}}}{|\mu_{21}^{(\text{diab})}|^4} \\
&= \sum_{\ell=1}^{N_{\text{traj}}} U_{22}\left(x^{(1)[\ell]}(\tau, t_0)\right) U_{22}\left(x^{(1)[\ell]}(t_0)\right) \exp\left[-\frac{i}{\hbar}\int_0^\tau d\tau'(\mathbb{E}_2(x^{(1)[\ell]}(\tau', t_0)) - \mathbb{E}_1(x^{(1)[\ell]}(\tau', t_0)))\right] \\
&+ \sum_{\ell=1}^{N_{\text{traj}}} U_{23}(x^{(1)[\ell]}(\tau, t_0)) U_{23}(x^{(1)[\ell]}(t_0)) \exp\left[-\frac{i}{\hbar}\int_0^\tau d\tau'(\mathbb{E}_3(x^{(1)[\ell]}(\tau', t_0)) - \mathbb{E}_1(x^{(1)[\ell]}(\tau', t_0)))\right],
\end{aligned}
\tag{15}
$$

where $\mathbb{E}_k(x)$ is the kth adiabatic potential, all trajectories are propagated on the ground adiabatic PES, and we have used the fact that $\mathbf{U}(x)$ is real for this system.

In the second approach, excited-state Kubo, the trajectories remain on the excited adiabats throughout the calculation of the electronic coherence. Specifically, the ℓth trajectory remains on its active surface at the end of the delay time, $\lambda^{[\ell]}(t_0)$, and is propagated using purely classical dynamics without allowing for any hops to other adiabatic PESs. The dipole-dipole correlation

This article is copyrighted as indicated in the article. Reuse of AIP content is subject to the terms at: http://scitation.aip.org/termsconditions. Downloaded to IP: 74.109.53.69 On: Mon, 27 Oct 2014 11:47:44

function is then calculated using

$$C_{\mu\mu}^{(\text{Kubo, }e)}(\tau, t_0)\frac{N_{\text{traj}}}{|\mu_{21}^{(\text{diab})}|^4}$$

$$= \sum_{\ell=1}^{N_{\text{traj}}} U_{22}(x^{[\ell]}(\tau, t_0))U_{22}(x^{[\ell]}(t_0)) \exp\left[-\frac{i}{\hbar}\int_0^{\tau'} d\tau'(\mathbb{E}_2(x^{[\ell]}(\tau', t_0)) - \mathbb{E}_1(x^{[\ell]}(\tau', t_0)))\right]\delta_{2,\lambda^{[\ell]}(t_0)}$$

$$+ \sum_{\ell=1}^{N_{\text{traj}}} U_{23}(x^{[\ell]}(\tau, t_0))U_{23}(x^{[\ell]}(t_0)) \exp\left[-\frac{i}{\hbar}\int_0^{\tau} d\tau'(\mathbb{E}_3(x^{[\ell]}(\tau', t_0)) - \mathbb{E}_1(x^{[\ell]}(\tau', t_0)))\right]\delta_{3,\lambda^{[\ell]}(t_0)}. \quad (16)$$

Finally, for the third approach, we consider the inhomogeneous limit of the spectra by constructing a histogram of the instantaneous distribution of energy gaps at each delay time weighted by the adiabatic transition dipole moments.[29,31,32,63] Specifically,

$$\frac{N_{\text{traj}}}{\left|\mu_{21}^{(\text{diab})}\right|^4}\frac{c}{4\omega\Delta}\alpha^{(\text{inh})}(\omega, t_0)$$

$$= \sum_{\ell=1}^{N_{\text{traj}}} \frac{|U_{22}(x^{[\ell]}(t_0))|^2}{(\mathbb{E}_2(x^{[\ell]}(t_0)) - \mathbb{E}_1(x^{[\ell]}(t_0)))^2 + (\Delta/2)^2}\delta_{2,\lambda^{[\ell]}(t_0)}$$

$$+ \sum_{\ell=1}^{N_{\text{traj}}} \frac{|U_{23}(x^{[\ell]}(t_0))|^2}{(\mathbb{E}_3(x^{[\ell]}(t_0)) - \mathbb{E}_1(x^{[\ell]}(t_0)))^2 + (\Delta/2)^2}\delta_{3,\lambda^{[\ell]}(t_0)}, \quad (17)$$

where $\Delta = 250\ \text{cm}^{-1}$ is a parameter used to approximate the lifetime broadening present in the other calculations due to the finite size of τ_{max}.

In the semiclassical calculations, we dynamically adjusted the size of the time step in order to ensure accurate integration of the equations of motion. Specifically, if the energy of a trajectory drifted significantly within a single time step, then the integration of the nuclear equations of motion over that time step was repeated using a series of smaller time steps to ensure energy conservation. Additionally, throughout the delay time – as well as when the coherences were evaluated using Eqs. (9) and (10) – we identified $h\nu_{\text{max}}$ as the magnitude of the largest element of the electronic Hamiltonian matrix in the time-dependent Schrödinger equation. If $(10\nu_{\text{max}})^{-1} < \delta t$ then integration of the electronic Schrödinger equation from t to $t + \delta t$ was performed over a series of smaller time steps of length $(10\nu_{\text{max}})^{-1}$. Note that regardless of the size of $(10\nu_{\text{max}})^{-1}$, hopping between electronic states was only considered at the end of the full time step from t to $t + \delta t$.

All semiclassical calculations performed in this study used an ensemble of 80 000 trajectories with the initial positions and momenta sampled from the Wigner distribution of the ground vibrational state on the ground PES.[78,79] The vibronic eigenstates required for the numerically exact quantum dynamics calculations were obtained using DVR in a sinc-DVR basis with a grid of 12 000 evenly spaced points spanning from −12 to 228 a.u. Note that the use of a very large grid was necessary to account for the fact that $V_3(x)$ is purely repulsive and that no artifacts associated with using a finite grid were observed over the time scales considered in the study. For all calculations, a time step of $\delta t = 0.05$ fs was used and the electronic coherences were propagated for $\tau_{\text{max}} = 100$ fs. The equations of motion in the semiclassical calculations were integrated using the fourth-order Runge Kutta algorithm.[82] The time-dependent differential absorbance spectra were calculated using Eq. (12) on a frequency grid containing 3695 evenly spaced points from 6000 cm^{-1} to 22 000 cm^{-1}.

Time-dependent differential absorbance spectra calculated using numerically exact quantum dynamics are shown as the solid black curves in Figure 4 for the three state model in the weak diabatic coupling limit ($V_{23} = 0.0001$ hartree). Note that the range of delay times shown cover two vibrational periods for $d = 1.0$ a.u. and one vibrational period for $d = 2.0$ a.u. The presence of excited state dynamics throughout the delay time is shown to have a pronounced impact on the spectral line shape, particularly with the larger value of horizontal shift, $d = 2.0$ a.u. When $V_{23} = 0.0001$ hartree, little change to the integrated intensity is evident, indicating that the dissociative dark state has only a minor impact on the excited state dynamics within the first one to two vibrational periods. However, as shown in Figure 5, when the diabatic coupling is increased by at least an order of magnitude to $V_{23} = 0.001$ hartree for $d = 1.0$ a.u. and $V_{23} = 0.002$ hartree for $d = 2.0$ a.u., the integrated intensity decreases markedly over the range of delay times considered in the study. This indicates that, for these larger diabatic couplings, strong nonadiabatic effects on the excited state dynamics result in a large transfer of population to the dark diabatic state within the first 100–200 fs following the pump pulse.

The results of semiclassical calculations performed using Eqs. (9) and (10) are shown as the dashed red lines in Figures 4 and 5. The underlying adiabatic and diabatic populations and norms of the dipole-dipole correlation functions are compared to the exact results in Figures S7–S9 in the supplementary material.[85] We Focus first on the weak diabatic coupling limit. The semiclassical calculations are shown to capture the overall evolution of the spectral envelope with increasing delay time as well as many of the underlying vibra-

This article is copyrighted as indicated in the article. Reuse of AIP content is subject to the terms at: http://scitation.aip.org/termsconditions. Downloaded to IP: 74.109.53.69 On: Mon, 27 Oct 2014 11:47:44

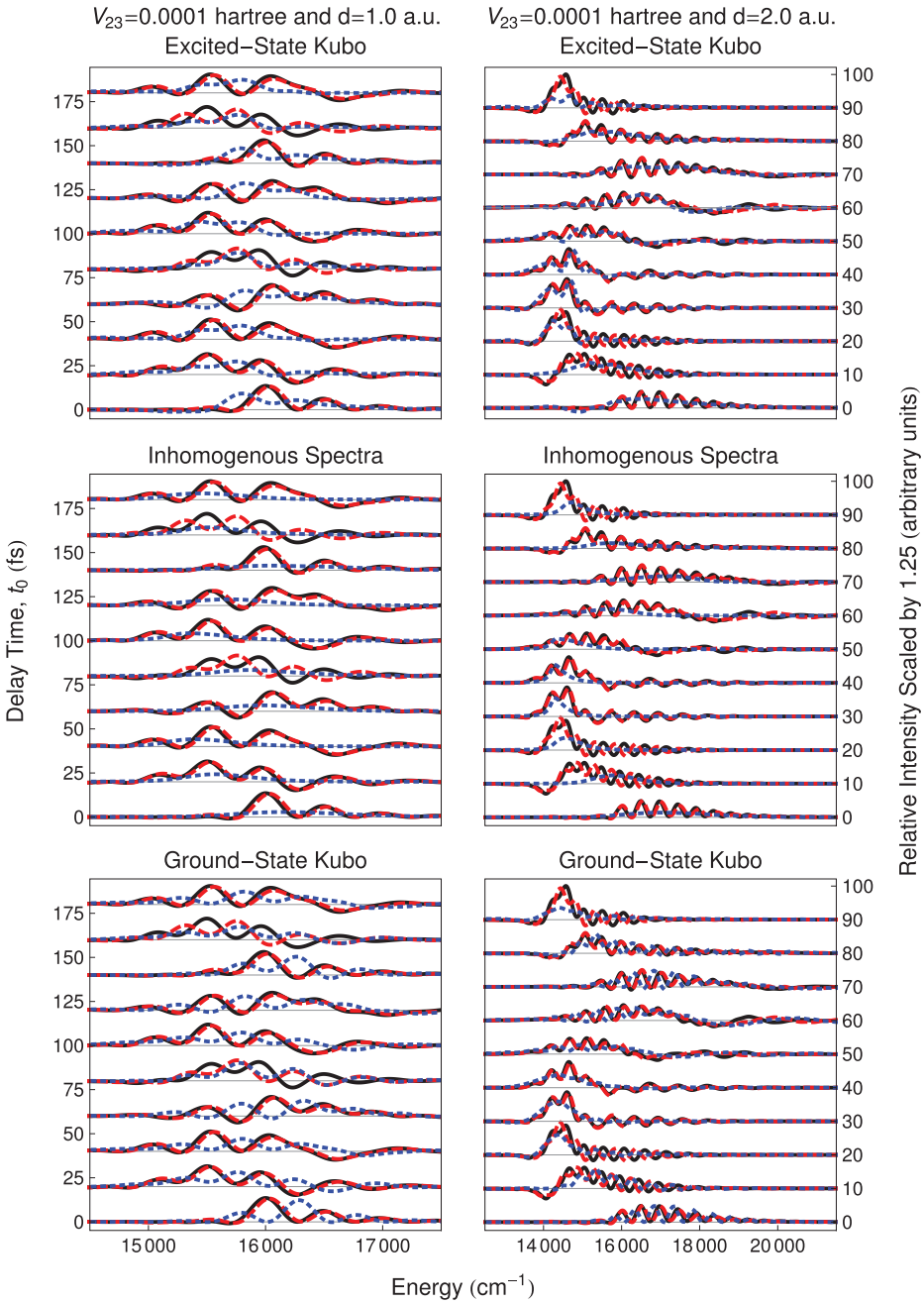


FIG. 4. A comparison between the time-dependent differential absorbance spectra of the three state model system defined by the diabats given in Eq. (13) with $V_{23} = 0.0001$ hartree and $d = 1.0$ a.u. or $d = 2.0$ a.u. The spectra are calculated using numerically exact quantum dynamics (solid black lines), semiclassically using Eqs. (9) and (10) (dashed red lines), and semiclassically using the alternative approaches given in Eqs. (15)–(17) (dotted blue lines).

tional features. While the deviations that are present in the semiclassical spectra are likely due to the neglect of nuclear quantum effects in our semiclassical calculations, it is not yet fully understood why the errors are more pronounced at certain values of t_0 than others.

Turning now to Figure 5, we increase the value of the diabatic coupling by at least an order of magnitude to $V_{23} = 0.001$ hartree for $d = 1.0$ a.u. and $V_{23} = 0.002$ hartree for $d = 2.0$ a.u. From the data, it is clear that the effects of significant nonadiabatic excited state dynamics on the time-dependent differential absorbance spectra are very well captured by Eqs. (9) and (10). Note that where deviations between the exact and semiclassical spectra occur, they tend to be more pronounced on the blue side of the line shapes and, as shown in greater detail in Figures S10–S24 in the supplementary material, involve the semiclassical calculations predicting too little intensity when V_{23} and t_0 are both large.[85]

Besides evaluating our suggested semiclassical ansatz, Figures 4 and 5 also show as the dotted blue lines the result of using the alternative semiclassical approaches discussed above (Eqs. (15)–(17)) to calculate the time-dependent differential absorbance spectra. The spectra calculated using the ground-state Kubo approach are in poor agreement with the exact spectra and fail to show a decrease in their

This article is copyrighted as indicated in the article. Reuse of AIP content is subject to the terms at: http://scitation.aip.org/termsconditions. Downloaded to IP: 74.109.53.69 On: Mon, 27 Oct 2014 11:47:44

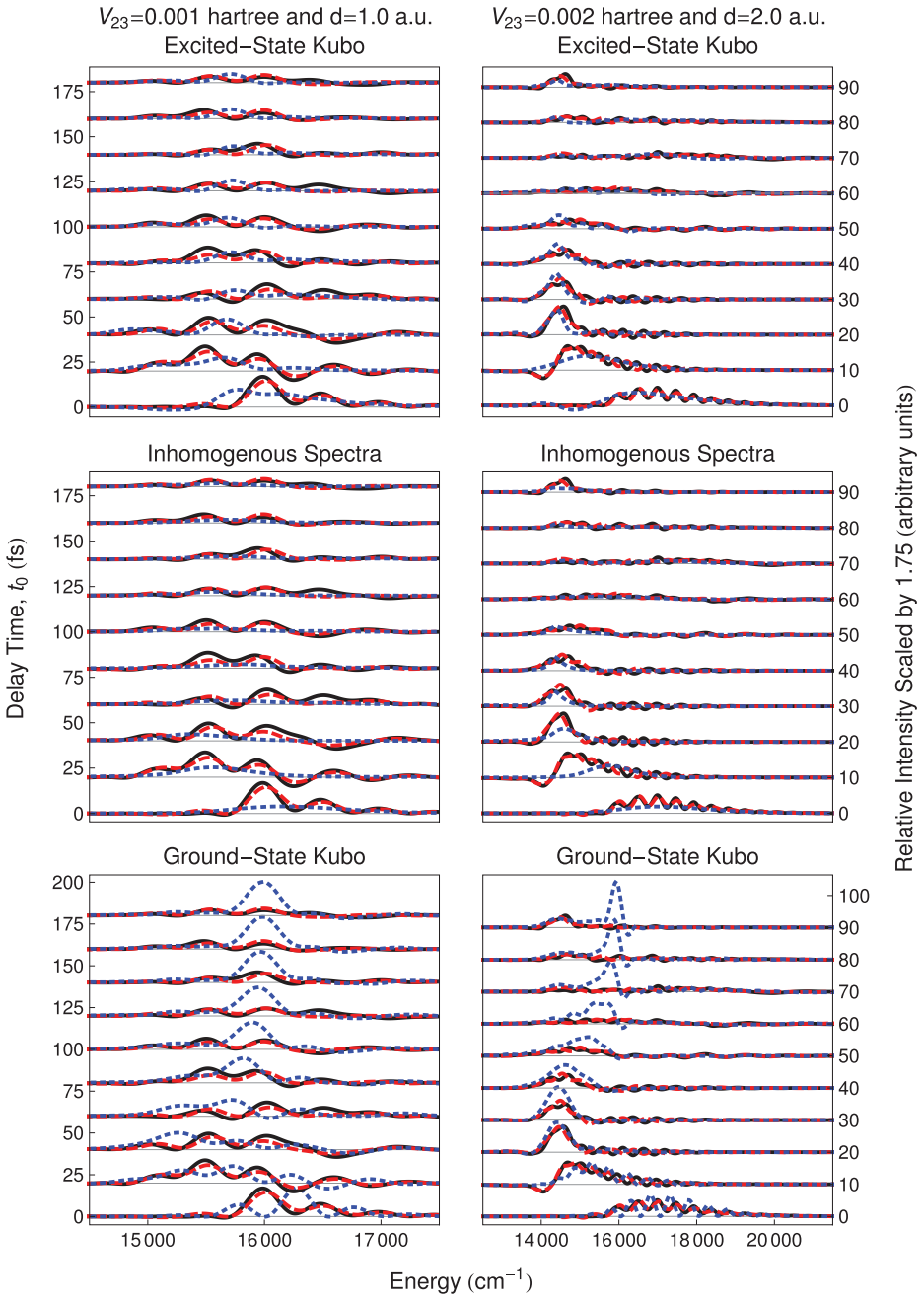


FIG. 5. A comparison between the time-dependent differential absorbance spectra of the three state model system defined by the diabats given in Eq. (13) with $V_{23} = 0.001$ hartree with $d = 1.0$ a.u. or $V_{23} = 0.002$ hartree with $d = 2.0$ a.u. The spectra are calculated using numerically exact quantum dynamics (solid black lines), semiclassically using Eqs. (9) and (10) (dashed red lines), and semiclassically using the alternative approaches given in Eqs. (15)–(17) (dotted blue lines).

integrated intensity as t_0 is increased when $V_{23} \geq 0.001$ hartree. Thus, Eq. (15) is unable to capture the key signature of nonadiabatic excited state dynamics in this model system. In contrast, the excited-state Kubo and inhomogenous limit spectra exhibit a decrease in the integrated intensity with increasing t_0 when the diabatic coupling is large. As such, Eqs. (16) and (17) are able to capture some qualitative effects of nonadiabatic wave packet dynamics, thus confirming one's obvious intuition that it is better to perform the dynamics on the excited adiabatic PESs than the ground PES during the evolution of the electronic coherence associated with stimulated emission. That being said, the spectra calculated using Eqs. (9) and (10) are consistently in better agreement with the exact spectra than the results of Eqs. (16) or (17). This demonstrates that including dynamical information from both the ground and excited states provides significant improvements to the semiclassical calculation of electronic spectra. Finally, note that a more complete data set for this model system can be found in Figures S10–S24 in the supplementary material.[85]

At this point, one caveat is in order. Figure 6 shows representative data illustrating the effect of increasing $\tau_{\max}$ on spectra calculated exactly and using the approach developed in this study. For the exact spectra, increasing the length of

This article is copyrighted as indicated in the article. Reuse of AIP content is subject to the terms at: http://scitation.aip.org/termsconditions. Downloaded to IP: 74.109.53.69 On: Mon, 27 Oct 2014 11:47:44

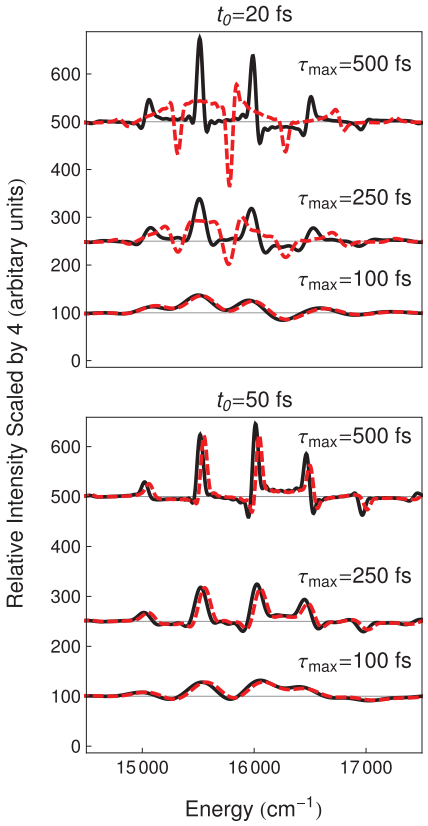


FIG. 6. Illustration of the dependence of the calculated spectra on how long the electronic coherences were propagated (τ_{max}). The results calculated using numerically exact quantum dynamics and semiclassically using Eqs. (9) and (10) are shown as the solid black lines and dashed red lines, respectively. Data are shown for the three state model system defined by the diabats given in Eq. (13) with $V_{23} = 0.001$ hartree and $d = 1.0$ a.u. at two representative delay times. The spectral intensities are scaled by a constant factor of 4. Note that the absorption spectra can become distorted for $\tau_{max} > 100$ fs, indicating that our approximations hold only for short times.

time over which the electronic coherence is propagated results in the expected sharpening of the spectral features. For some delay times, as shown in the bottom panel of Figure 6, the same is true for the spectra calculated using Eqs. (9) and (10). However, for other delay times, as shown in the top panel of Figure 6, the semiclassical spectra develop large errors as τ_{max} is increased. This behavior reflects the fact that Eqs. (9) and (10) represent a short-time approximation to the Quantum-Classical Liouville Equation of Kapral and Martens, as discussed in Appendix B of our previous study.[58] As such, our FSSH calculation of electronic coherences can develop errors at long times, with Figure 6 indicating that the extent to which this occurs depends on the specific initial conditions of the coherence. Importantly, as originally argued by Heller, the semiclassical calculation of electronic spectral line shapes requires the evaluation of correlation functions over only short times, usually only 1–5 fs if the overall Franck-Condon envelope is all that is required.[40] Indeed, as evident in Figures 4 and 5, the electronic coherences calculated using Eqs. (9) and (10) are clearly stable over sufficiently long timescales to allow the overall spectral envelopes as well as vibrational structure to be captured in the semiclassical spectra. Thus, while unfortunate, the errors evident in Figure 6 when $\tau_{max} > 100$ fs are not catastrophic. In fact, they might not even be evident for condensed phase problems due to the fast decay of the coherences resulting from interactions with the environment.

Finally, the reader may be curious about the effect of including decoherence during the calculation of the spectra using Eqs. (9) and (10). We explored this question by using our group's augmented-FSSH (AFSSH) algorithm to propagate the mixed quantum-classical trajectories instead of FSSH.[69,71,77] We tried several ways of implementing this. First, we found that if decoherence is introduced between all of the electronic states, then the spectroscopically relevant electronic coherences decay to zero much too quickly, resulting in an unphysical spectral broadening. Second, introducing decoherence between just the excited states for all times $t > 0$ results in the loss of vibrational structure in the calculated spectra, although the overall spectral envelopes are still captured. As third and final alternative, we considered introducing decoherence effects between the excited states only during the evolution of the excited state populations during the delay time ($t < t_0$), with FSSH used to propagate the electronic coherences for $t > t_0$. Although this did improve the agreement between the semiclassical and exact adiabatic and diabatic populations, as shown in Figures S7 and S8 of the supplementary material, the spectra calculated using this scheme are found to be comparable to those calculated using only FSSH. Examples of this analysis can be found in Figures S10–S24 in the supplementary material.[85] Overall, the basic premise of introducing decoherence in FSSH is that separating wave packets do not recombine. Since the waxing and waning of wave packet overlaps is clearly essential for modeling spectra from time correlation functions (with many cycles necessary in the gas phase), adding decoherence is either not appropriate or not very useful here.

IV. CONCLUSIONS

In this paper, we have described a semiclassical approach for calculating full time-dependent differential absorbance line shapes (beyond the inhomogeneous component) associated with pump-probe spectroscopy in the limit of ultrashort pulses. We use ensembles of FSSH trajectories that are first propagated on the excited surface(s) throughout the delay time between the pulses. At the onset of the probe pulse, the electronic coherence is modeled using two ensembles of mixed quantum-classical trajectories that are initialized on the ground and excited PESs. Dynamical information from both of these ensembles is averaged together to obtain the overall optical response function. In the absence of electronic relaxation, we have shown that our approach is exact for the model problem of two shifted harmonic potentials with identical harmonic frequencies and outperforms both ground- and excited-state Kubo when the harmonic frequencies differ. Using a model three state system in which a bright excited state is vibronically coupled to a repulsive dark state, we demonstrated that our approach is able to capture the signatures of nonadiabatic excited state dynamics on the time-dependent differential absorbance spectra. Moreover, our approach significantly outperforms ground-state Kubo, excited-state Kubo, and the

This article is copyrighted as indicated in the article. Reuse of AIP content is subject to the terms at: http://scitation.aip.org/termsconditions. Downloaded to IP: 74.109.53.69 On: Mon, 27 Oct 2014 11:47:44

inhomogeneous calculation of the spectra. Although we have focused on stimulated emission in this study, Eqs. (9) and (10) can be directly applied to excited state absorption by simply replacing the ground state with the appropriate additional excited state(s) encountered during the evolution of the electronic coherence.

As emphasized earlier, note that all of the model systems considered in this study are gas phase with only a single nuclear degree of freedom. As a result, there are no environmental interactions or multiple vibrational degrees of freedom with which to damp out the long-time oscillations of $C_{\mu\mu}(t)$. This is particularly important in the limit of small V_{23} where bound-state dynamics are dominant and the dipole-dipole correlation will decay very slowly. Moreover, the time dependence of $C_{\mu\mu}(t)$ is dependent on the details of the repeated separation and recombination of wave packets moving on different surfaces and therefore will be sensitive to nuclear quantum effects, such as decoherences and recoherences, which cannot be fully captured by swarms of non-interacting FSSH trajectories. Despite these challenges, Eqs. (9) and (10) are shown to be capable of capturing the signatures of nonadiabatic excited state dynamics in the time-dependent differential absorbance spectra as well as (surprisingly) much of the underlying vibrational structure in the spectral line shapes. As a result, we expect that our approach will provide a useful tool for modeling coherent pump-probe electronic spectroscopy in condensed phase systems. More generally, we have shown that ensembles of FSSH trajectories can be used to propagate electronic coherences with non-stationary initial conditions, a situation that appears in many other areas of nonlinear spectroscopy. Efforts to generalize the ideas developed in this study to three-pulse experiments, as in multi-dimensional electronic spectroscopy, are currently underway in our lab. Additionally, we are working on extending the approach to systems that include nonadiabatic couplings between the ground and excited states as well as to model condensed phase problems. Finally, in a future paper we will also benchmark the current approach against Ehrenfest dynamics.

ACKNOWLEDGMENTS

This material is based upon work supported by the (U.S.) Air Force Office of Scientific Research (USAFOSR) PECASE award under AFOSR Grant No. FA9950-13-1-0157. J.E.S. acknowledges a Cottrell Research Scholar Fellowship and a David and Lucille Packard Fellowship. We thank the Journal of Chemical Physics reviewers for their insightful comments on this work.

APPENDIX A: EQUATION (6) IS EXACT FOR TWO UNCOUPLED, SHIFTED HARMONIC POTENTIALS WITH IDENTICAL HARMONIC FREQUENCIES

We consider the shifted harmonic potentials model of Eq. (11) with $\omega_g = \omega_e = \omega$. As discussed above, the nonlinear optical response function associated with the time- and frequency-resolved stimulated emission spectra of a coherent pump-probe experiment in the limit of ultrashort pulses can be written as[7,14,15,38]

$$\begin{aligned} C_{\mu\mu}(\tau, t_0) &= \langle 0|\hat{\mu}_{ge} \exp[i\hat{H}_e t_0/\hbar]\hat{\mu}_{eg} \exp[i\hat{H}_g \tau/\hbar]\hat{\mu}_{ge} \\ &\quad \times \exp[-i\hat{H}_e(\tau + t_0)/\hbar]\hat{\mu}_{eg}|0\rangle \\ &= |\mu_{eg}|^4 \langle 0| \exp[i\hat{H}_e t_0/\hbar] \exp[i\hat{H}_g \tau/\hbar] \\ &\quad \times \exp[-i\hat{H}_e(\tau + t_0)/\hbar]|0\rangle, \end{aligned} \tag{A1}$$

where $\tau = t - t_0$, in the second line we have assumed the Condon approximation, and prior to the pump pulse, the system is assumed to be in the ground vibrational state on the ground PES. Noting that $\hat{H}_g$ and $\hat{H}_e$ are related by $\hat{D}^\dagger \hat{H}_g \hat{D} + \epsilon_0 = \hat{H}_e$, where $\hat{D} = \exp[-i\hat{p}d/\hbar]$ is the shift operator,[47] we can rewrite Eq. (A1) as

$$\begin{aligned} \frac{C_{\mu\mu}(\tau, t_0)}{|\mu_{eg}|^4} &= e^{-i\epsilon_0\tau/\hbar}\langle 0|\hat{D}^\dagger \exp[i\hat{H}_g t_0/\hbar]\hat{D} \exp[i\hat{H}_g \tau/\hbar]\hat{D}^\dagger \\ &\quad \times \exp[-i\hat{H}_g(t_0 + \tau)/\hbar]\hat{D}|0\rangle \\ &= e^{-i\epsilon_0\tau/\hbar}\langle 0|\hat{D}^\dagger \hat{D}(t_0)\hat{D}^\dagger(t_0 + \tau)\hat{D}|0\rangle. \end{aligned} \tag{A2}$$

To make progress, we use the relationship between the momentum operator and the harmonic oscillator raising and lowering operators,

$$\hat{p}(t) = \frac{i\sqrt{m\omega\hbar}}{\sqrt{2}}(\hat{a}^\dagger e^{i\omega t} - \hat{a}e^{-i\omega t}), \tag{A3}$$

to write

$$\begin{aligned} \hat{D}(t) &= \exp\left[d\sqrt{\frac{m\omega}{2\hbar}}(\hat{a}^\dagger e^{i\omega t} - \hat{a}e^{-i\omega t})\right] \\ &= \exp[\tilde{d}(\hat{a}^\dagger e^{i\omega t} - \hat{a}e^{-i\omega t})], \end{aligned} \tag{A4}$$

where $\tilde{d} = d\sqrt{m\omega/2\hbar}$. We can then use the identity $e^{\hat{A}+\hat{B}} = e^{\hat{A}}e^{\hat{B}}e^{-[\hat{A},\hat{B}]/2}$, which holds provided $\hat{A}$ and $\hat{B}$ both commute with $[\hat{A}, \hat{B}]$,[47] to write

$$\begin{aligned} \hat{D}(t) &= \exp[\tilde{d}\hat{a}^\dagger e^{i\omega t}] \exp[-\tilde{d}\hat{a}e^{-i\omega t}] \exp[-\tilde{d}^2/2] \\ &= \exp[-\tilde{d}\hat{a}e^{-i\omega t}] \exp[\tilde{d}\hat{a}^\dagger e^{i\omega t}] \exp[\tilde{d}^2/2]. \end{aligned} \tag{A5}$$

Using these results and the identity $e^{\hat{A}}e^{\hat{B}} = e^{\hat{B}}e^{\hat{A}}e^{-[\hat{B},\hat{A}]}$ we can simplify Eq. (A2) as

$$\begin{aligned} \frac{C_{\mu\mu}(\tau, t_0)}{|\mu_{eg}|^4} &= e^{-i\epsilon_0\tau/\hbar}\langle 0| \exp[-\tilde{d}\hat{a}^\dagger] \exp[\tilde{d}\hat{a}] \exp[-\tilde{d}^2/2] \exp[-\tilde{d}\hat{a}e^{-i\omega t_0}] \exp[\tilde{d}\hat{a}^\dagger e^{i\omega t_0}] \\ &\quad \times \exp[\tilde{d}^2/2] \exp[-\tilde{d}\hat{a}^\dagger e^{i\omega(t_0+\tau)}] \exp[\tilde{d}\hat{a}e^{-i\omega(t_0+\tau)}] \exp[-\tilde{d}^2/2] \\ &\quad \times \exp[-\tilde{d}\hat{a}] \exp[\tilde{d}\hat{a}^\dagger] \exp[\tilde{d}^2/2]|0\rangle \end{aligned}$$

This article is copyrighted as indicated in the article. Reuse of AIP content is subject to the terms at: http://scitation.aip.org/termsconditions. Downloaded to IP: 74.109.53.69 On: Mon, 27 Oct 2014 11:47:44

$$
\begin{aligned}
&= e^{-i\epsilon_0\tau/\hbar}\langle 0|\exp[-\tilde{d}\hat{a}^\dagger]\exp[\tilde{d}\hat{a}(1-e^{-i\omega t_0})]\exp[\tilde{d}\hat{a}^\dagger e^{i\omega t_0}(1-e^{i\omega\tau})]\\
&\quad\times\exp[\tilde{d}\hat{a}(e^{-i\omega(t_0+\tau)}-1)]\exp[\tilde{d}\hat{a}^\dagger]|0\rangle\\
&= e^{-i\epsilon_0\tau/\hbar}\langle 0|\exp[\tilde{d}\hat{a}^\dagger e^{i\omega t_0}(1-e^{i\omega\tau})]\exp[\tilde{d}\hat{a}(1-e^{-i\omega t_0})]\\
&\quad\times\exp[-\tilde{d}^2 e^{i\omega t_0}(1-e^{i\omega\tau})(1-e^{-i\omega t_0})[\hat{a}^\dagger,\hat{a}]]\\
&\quad\times\exp[\tilde{d}\hat{a}(e^{-i\omega(t_0+\tau)}-1)]\exp[\tilde{d}\hat{a}^\dagger]|0\rangle\\
&= e^{-i\epsilon_0\tau/\hbar}\exp[\tilde{d}^2 e^{i\omega t_0}(1-e^{i\omega\tau})(1-e^{-i\omega t_0})]\\
&\quad\times\langle 0|\exp[\tilde{d}\hat{a}(1-e^{-i\omega t_0}+e^{-i\omega(t_0+\tau)}-1)]\exp[\tilde{d}\hat{a}^\dagger]|0\rangle\\
&= e^{-i\epsilon_0\tau/\hbar}\exp[\tilde{d}^2 e^{i\omega t_0}(1-e^{i\omega\tau})(1-e^{-i\omega t_0})]\\
&\quad\times\langle 0|\exp[\tilde{d}\hat{a}^\dagger]\exp[\tilde{d}\hat{a}(e^{-i\omega(t_0+\tau)}-e^{-i\omega t_0})]\exp[-\tilde{d}^2(e^{-i\omega(t_0+\tau)}-e^{-i\omega t_0})[\hat{a}^\dagger,\hat{a}]]|0\rangle\\
&= e^{-i\epsilon_0\tau/\hbar}\exp[\tilde{d}^2(e^{i\omega t_0}(1-e^{i\omega\tau})(1-e^{-i\omega t_0})+e^{-i\omega(t_0+\tau)}-e^{-i\omega t_0})]\\
&= e^{-i\epsilon_0\tau/\hbar}\exp[i\tilde{d}^2(2\sin(\omega t_0)-2\sin(\omega(t_0+\tau))+\sin(\omega\tau))]\exp[\tilde{d}^2(\cos(\omega\tau)-1)].
\end{aligned}
\tag{A6}
$$

We now turn to the semiclassical description of the process using Eq. (6). We will focus first on the swarm of trajectories that remain on the excited potential throughout the calculation. Each trajectory propagated on the excited PES with initial conditions (x_0, p_0) satisfies

$$
x^{(e)}(t) = d + (x_0 - d)\cos(\omega t) + \frac{p_0}{m\omega}\sin(\omega t). \tag{A7}
$$

The electronic coherence associated with this ensemble is calculated according to Eq. (4) as

$$
\begin{aligned}
\frac{\langle\sigma_{eg}^{(e)}(t,t_0)\rangle_{t_0}}{\sigma_{eg}(t_0)} &= \left\langle\exp\left[-\frac{i}{\hbar}\int_{t_0}^{t}(H_e(\vec{x}^{\,(e)}(t'),\vec{p}^{\,(e)}(t')) - H_g(\vec{x}^{\,(e)}(t'),\vec{p}^{\,(e)}(t')))dt'\right]\right\rangle_{t_0}\\
&= \left\langle\exp\left[-\frac{i}{\hbar}\int_{t_0}^{t}\left\{\epsilon_0 - \frac{m\omega^2 d}{2}\left(d - 2d\cos(\omega t') + 2x_0\cos(\omega t') + \frac{2p_0}{m\omega}\sin(\omega t')\right)\right\}dt'\right]\right\rangle_{t_0}\\
&= \exp\left[-\frac{i\epsilon_0(t-t_0)}{\hbar} + \frac{im\omega^2 d^2(t-t_0)}{2\hbar} - \frac{im\omega d^2(\sin(\omega t)-\sin(\omega t_0))}{\hbar}\right]\\
&\quad\times\left\langle\exp\left[-\frac{i}{\hbar}\Big(dp_0(\cos(\omega t)-\cos(\omega t_0)) - m\omega d x_0(\sin(\omega t)-\sin(\omega t_0))\Big)\right]\right\rangle_{t_0}.
\end{aligned}
\tag{A8}
$$

Averaging over the initial conditions that are sampled from the harmonic oscillator ground state Wigner distribution is accomplished according to

$$
\begin{aligned}
&\left\langle\exp\left[-\frac{i}{\hbar}(dp_0(\cos(\omega t)-\cos(\omega t_0)) - m\omega d x_0(\sin(\omega t)-\sin(\omega t_0))\right]\right\rangle_{t_0}\\
&= \frac{1}{\pi\hbar}\int_{-\infty}^{\infty}dp_0\exp\left[-\frac{ip_0 d}{\hbar}(\cos(\omega t)-\cos(\omega t_0))\right]\exp\left[-\frac{p_0^2}{m\omega\hbar}\right]\\
&\quad\times\int_{-\infty}^{\infty}dx_0\exp\left[\frac{im\omega x_0 d}{\hbar}(\sin(\omega t)-\sin(\omega t_0))\right]\exp\left[-\frac{m\omega x_0^2}{\hbar}\right]\\
&= \exp\left[-\frac{m\omega d^2}{4\hbar}(\sin(\omega t)-\sin(\omega t_0))^2\right]\exp\left[-\frac{m\omega d^2}{4\hbar}(\cos(\omega t)-\cos(\omega t_0))^2\right]\\
&= \exp\left[-\frac{m\omega d^2}{2\hbar}(1-\cos(\omega(t-t_0)))\right]\\
&= \exp\left[-\frac{m\omega d^2}{2\hbar}(1-\cos(\omega\tau))\right].
\end{aligned}
\tag{A9}
$$

This article is copyrighted as indicated in the article. Reuse of AIP content is subject to the terms at: http://scitation.aip.org/termsconditions. Downloaded to IP: 74.109.53.69 On: Mon, 27 Oct 2014 11:47:44

Therefore, the full semiclassical expression for the coherence obtained from the trajectories moving on the excited potential is given by

$$\left\langle \sigma_{eg}^{(e)}(\tau, t_0)\right\rangle_{t_0} = \sigma_{eg}(t_0)\exp\left[-\frac{m\omega d^2}{2\hbar}(1-\cos(\omega\tau))\right] \times \exp\left[-\frac{i\epsilon_0\tau}{\hbar} + \frac{im\omega^2 d^2\tau}{2\hbar} - \frac{im\omega d^2}{\hbar}\sin(\omega(\tau+t_0)) + \frac{im\omega d^2}{\hbar}\sin(\omega t_0)\right]. \tag{A10}$$

We now turn to the swarm of trajectories that are evolving on the ground surface during the period over which the electronic coherence is calculated. At the onset of the electronic coherence at $t = t_0$, these trajectories have positions and momenta

$$\begin{aligned} x(t_0) &= d + (x_0 - d)\cos(\omega t_0) + \frac{p_0}{m\omega}\sin(\omega t_0), \\ p(t_0) &= -m\omega(x_0 - d)\sin(\omega t_0) + p_0\cos(\omega t_0). \end{aligned} \tag{A11}$$

After one of these trajectories has evolved on the ground state for a period of time τ, its position is

$$x(\tau) = \left(d + (x_0 - d)\cos(\omega t_0) + \frac{p_0}{m\omega}\sin(\omega t_0)\right)\cos(\omega\tau) + \left((d - x_0)\sin(\omega t_0) + \frac{p_0}{m\omega}\cos(\omega t_0)\right)\sin(\omega\tau). \tag{A12}$$

Focusing on the time integral in Eq. (3) and using the expression for the time-dependent positions of the trajectories given in Eq. (A12) we have

$$\begin{aligned} &\int_0^\tau (H_e(\vec{x}^{\,(g)}(\tau', t_0), \vec{p}^{\,(g)}(\tau', t_0)) - H_g(\vec{x}^{\,(g)}(\tau', t_0), \vec{p}^{\,(g)}(\tau', t_0)))d\tau' \\ &= \int_0^\tau \left(\epsilon_0 + \frac{m\omega^2 d^2}{2} - \frac{m\omega^2}{2}2d\left(d + (x_0 - d)\cos(\omega t_0) + \frac{p_0}{m\omega}\sin(\omega t_0)\right)\cos(\omega\tau')\right)d\tau' \\ &\quad + \int_0^\tau \left(-\frac{m\omega^2}{2}2d\left((d - x_0)\sin(\omega t_0) + \frac{p_0}{m\omega}\cos(\omega t_0)\right)\sin(\omega\tau')\right)d\tau' \\ &= \epsilon_0\tau + \frac{m\omega^2 d^2}{2}\tau - m\omega^2 d\left(d + (x_0 - d)\cos(\omega t_0) + \frac{p_0}{m\omega}\sin(\omega t_0)\right)\frac{\sin(\omega\tau)}{\omega} \\ &\quad + -m\omega^2 d\left((d - x_0)\sin(\omega t_0) + \frac{p_0}{m\omega}\cos(\omega t_0)\right)\left(\frac{1-\cos(\omega\tau)}{\omega}\right) \\ &= \epsilon_0\tau + \frac{m\omega^2 d^2}{2}\tau - m\omega d^2\sin(\omega\tau) - m\omega d^2\sin(\omega t_0) + m\omega d^2\sin(\omega(t_0+\tau)) \\ &\quad + x_0 m\omega d(\sin(\omega t_0) - \sin(\omega(t_0+\tau))) - p_0 d(\cos(\omega t_0) - \cos(\omega(t_0+\tau))). \end{aligned} \tag{A13}$$

The semiclassical approximation to the electronic coherence is thus

$$\langle \sigma_{eg}^{(g)}(\tau, t_0)\rangle_{t_0} = \sigma_{eg}(t_0)\exp\left[-\frac{m\omega d^2}{2\hbar}(1-\cos(\omega\tau))\right] \times \exp\left[-\frac{i}{\hbar}\left(\epsilon_0\tau + \frac{m\omega^2 d^2}{2}\tau - m\omega d^2\sin(\omega\tau) - m\omega d^2\sin(\omega t_0) + m\omega d^2\sin(\omega(t_0+\tau))\right)\right], \tag{A14}$$

where the averaging over initial conditions was accomplished as in Eq. (A9).

Combining Eqs. (A10) and (A14) using Eq. (6) results in

$$C_{\mu\mu}^{(\mathrm{SC})}(\tau, t_0) = \exp\left[-\frac{m\omega d^2}{2\hbar}(1-\cos(\omega\tau))\right] \times \exp\left[-\frac{i}{2\hbar}\left(\epsilon_0\tau + \frac{m\omega^2 d^2}{2}\tau - m\omega d^2\sin(\omega\tau) - m\omega d^2\sin(\omega t_0) + m\omega d^2\sin(\omega(t_0+\tau))\right)\right]$$

This article is copyrighted as indicated in the article. Reuse of AIP content is subject to the terms at: http://scitation.aip.org/termsconditions. Downloaded to IP: 74.109.53.69 On: Mon, 27 Oct 2014 11:47:44

$$\times \exp\left[-\frac{i}{2\hbar}\left(\epsilon_0\tau - \frac{m\omega^2 d^2}{2}\tau + m\omega d^2\sin(\omega(\tau+t_0)) - m\omega d^2\sin(\omega t_0)\right)\right]$$

$$= \exp\left[\tilde{d}^2(\cos(\omega\tau)-1)\right]\exp\left[-\frac{i\epsilon_0\tau}{\hbar} + i\tilde{d}^2(2\sin(\omega t_0)+\sin(\omega\tau)-\sin(\omega(t_0+\tau))\right]. \quad \text{(A15)}$$

Comparing Eq. (A15) to Eq. (A6), we see that, for this model system, the results of our semiclassical approach are in exact agreement with the results of exact quantum dynamics.

APPENDIX B: GENERALIZING EQS. (9) AND (10) TO APPROXIMATELY ACCOUNT FOR NON-CONDON EFFECTS AND MULTIPLE BRIGHT STATES IN THE DIABATIC REPRESENTATION

Note that, starting with a mixed quantum-classical density matrix in the Wigner representation, one cannot easily and efficiently calculate dipole-dipole correlation functions for systems that are non-Condon in all representations; such calculations formally involve evaluating highly oscillatory integrals that will be difficult to converge. That being said, if we make approximations based on a classical expansion of the dynamics, then we can generalize Eqs. (9) and (10) to account for the spatially varying transition dipole moments that arise for most (non-Condon) chemical systems. The natural generalization of Eq. (10) is

$$C^{(\text{diab})}_{\mu\mu}(\tau,t_0) = \sqrt{\left\langle C^{(\text{diab},g)}_{\mu\mu}(\tau,t_0)\right\rangle\left\langle C^{(\text{diab},e)}_{\mu\mu}(\tau,t_0)\right\rangle}. \quad \text{(B1)}$$

Here, $\langle C^{(\text{diab},g)}_{\mu\mu}(\tau,t_0)\rangle$ and $\langle C^{(\text{diab},e)}_{\mu\mu}(\tau,t_0)\rangle$ are dipole-dipole correlation functions calculated using ensembles of FSSH trajectories propagated on the ground and excited adiabats, respectively, e.g.,

$$\begin{aligned}\left\langle C^{(\text{diab},e)}_{\mu\mu}(\tau,t_0)\right\rangle = \frac{1}{N_{\text{traj}}}\sum_{k=1}^{N_{\text{bright}}}\sum_{\ell=1}^{N_{\text{traj}}}&\mu^{(\text{diab})}_{k1}(x^{[\ell]}(\tau,t_0))\mu^{(\text{diab})}_{1k}(x^{[\ell]}(t_0))\left|\mu^{(\text{diab})}_{\lambda^{[\ell]}(0)1}(x^{[\ell]}(0))\right|^2\\ &\times\left[\sum_{mn}U_{km}(x^{[\ell]}(\tau,t_0))U^*_{1n}(x^{[\ell]}(\tau,t_0))\frac{\sigma^{[\ell]}_{mn}(\tau,t_0)}{\sigma^{[\ell]}_{mm}(\tau,t_0)+\sigma^{[\ell]}_{nn}(\tau,t_0)}(\delta_{m\lambda^{[\ell]}(\tau,t_0)}+\delta_{n\lambda^{[\ell]}(\tau,t_0)})\right]\\ &\times\left[\sum_{mn}U_{km}(x^{[\ell]}(t_0))U^*_{1n}(x^{[\ell]}(t_0))\frac{\sigma^{[\ell]}_{mn}(t_0)}{\sigma^{[\ell]}_{mm}(t_0)+\sigma^{[\ell]}_{nn}(t_0)}(\delta_{m\lambda^{[\ell]}(t_0)}+\delta_{n\lambda^{[\ell]}(t_0)})\right]. \quad \text{(B2)}\end{aligned}$$

Note that Eq. (B2) is a generalization of Eq. (9) and is valid for arbitrarily many bright diabatic states, $N_{\text{bright}} \geq 1$, without any additional approximations. It is also important to note that Eq. (B1) still assumes that no nonadiabatic couplings exist between the ground state and any of the excited states.

[1] *Femtosecond Chemistry*, edited by J. Manz and L. Wöste (VCH, New York, 1995).
[2] A. H. Zewail, *Femtochemistry – Ultrafast Dynamics of the Chemical Bond* (World Scientific, Singapore, 1994).
[3] J. P. Ogilvie and K. J. Kubarych, Adv. Atom. Mol. Opt. Phys. **57**, 249 (2009).
[4] M. Cho, Chem. Rev. **108**, 1331 (2008).
[5] J. Chen and B. Kohler, J. Am. Chem. Soc. **136**, 6362 (2014).
[6] R. Berera, R. van Grondelle, and J. T. M. Kennis, Photosynth. Res. **101**, 105 (2009).
[7] D. J. Tannor, *Introduction to Quantum Mechanics: A Time Dependent Perspective* (University Science Press, Sausalito, 2007).
[8] S. Mukamel, *Principles of Nonlinear Optical Spectroscopy* (Oxford University Press, 1995).
[9] N. K. Schwalb, R. Siewertsen, F. Renth, and F. Temps, in *Conical Intersections: Theory, Computation, and Experiment*, edited by W. Domcke, D. R. Yarkony, and H. Köppel (World Scientific Publishing Co. Pte. Ltd., 2011), pp. 669–714.
[10] W. K. Peters, E. R. Smith, and D. M. Jonas, in *Conical Intersections: Theory, Computation, and Experiment*, edited by W. Domcke, D. R. Yarkony, and H. Köppel (World Scientific Publishing Co. Pte. Ltd., 2011), pp. 715–746.
[11] M. Liebel, C. Schnedermann, G. Bassolino, G. Taylor, A. Watts, and P. Kukura, Phys. Rev. Lett. **112**, 238301 (2014).
[12] J. Li, Z. Nie, Y. Y. Zheng, S. Dong, and Z.-H. Loh, J. Phys. Chem. Lett. **4**, 3698 (2013).
[13] C. Y. Wong, S. B. Penwell, B. L. Cotts, R. Noriega, H. Wu, and N. S. Ginsberg, J. Phys. Chem. C **117**, 22111 (2013).
[14] W. T. Pollard, S.-Y. Lee, and R. A. Mathies, J. Chem. Phys. **92**, 4012 (1990).
[15] W. T. Pollard and R. A. Mathies, Annu. Rev. Phys. Chem. **43**, 497 (1992).
[16] L. Seidner, G. Stock, and W. Domcke, J. Chem. Phys. **103**, 3998 (1995).
[17] M. F. Gelin, A. V. Pisliakov, D. Egorova, and W. Domcke, J. Chem. Phys. **118**, 5287 (2003).
[18] M. F. Gelin, D. Egorova, and W. Domcke, Chem. Phys. **312**, 135 (2005).
[19] S. Dilthey, S. Hahn, and G. Stock, J. Chem. Phys. **112**, 4910 (2000).
[20] Q. Shi and E. Geva, J. Chem. Phys. **122**, 064506 (2005).
[21] P. L. McRobbie and E. Geva, J. Phys. Chem. A **113**, 10425 (2009).
[22] N. E. Shemetulskis and R. F. Loring, J. Chem. Phys. **97**, 1217 (1992).
[23] R. Tempelaar, C. P. van der Vegte, J. Knoester, and T. L. C. Jansen, J. Chem. Phys. **138**, 164106 (2013).
[24] C. P. van der Vegte, A. G. Dijkstra, J. Knoester, and T. L. C. Jansen, J. Phys. Chem. A **117**, 5970 (2013).
[25] V. S. Batista, M. T. Zanni, B. J. Greenblatt, D. M. Neumark, and W. H. Miller, J. Chem. Phys. **110**, 3736 (1999).

This article is copyrighted as indicated in the article. Reuse of AIP content is subject to the terms at: http://scitation.aip.org/termsconditions. Downloaded to IP: 74.109.53.69 On: Mon, 27 Oct 2014 11:47:44

[26]B. J. Ka and E. Geva, J. Chem. Phys. **125**, 214501 (2006).
[27]N. Rekik, C.-Y. Hsieh, H. Freedman, and G. Hanna, J. Chem. Phys. **138**, 144106 (2013).
[28]F. Webster, J. Schnitker, M. Friedrichs, R. A. Friesner, and P. J. Rossky, Phys. Rev. Lett. **66**, 3172 (1991).
[29]B. J. Schwartz and P. J. Rossky, J. Chem. Phys. **101**, 6917 (1994).
[30]H. R. Hudock, B. G. Levine, A. L. Thompson, H. Satzger, D. Townsend, N. Gador, S. Ullrich, A. Stolow, and T. J. Martínez, J. Phys. Chem. A **111**, 8500 (2007).
[31]R. Mitrić, U. Werner, and V. Bonačić-Koutecký, J. Chem. Phys. **129**, 164118 (2008).
[32]A. Humeniuk, M. Wohlgemuth, T. Suzuki, and R. Mitrić, J. Chem. Phys. **139**, 134104 (2013).
[33]R. Kubo, Adv. Chem. Phys. **15**, 101 (1969).
[34]A. Stolow, Annu. Rev. Phys. Chem. **54**, 89 (2003).
[35]A. Stolow, A. E. Bragg, and D. M. Neumark, Chem. Rev. **104**, 1719 (2004).
[36]T. Suzuki, Annu. Rev. Phys. Chem. **57**, 555 (2006).
[37]Q. Wang, R. W. Schoenlein, L. A. Peteanu, R. A. Mathies, and C. V. Shank, Science **266**, 422 (1994).
[38]S.-Y. Lee, in *Femtosecond Chemistry*, edited by J. Manz and L. Wöste (VCH, 1995).
[39]R. Coalson, D. G. Evans, and A. Nitzan, J. Chem. Phys. **101**, 436 (1994).
[40]E. J. Heller, Acc. Chem. Res. **14**, 368 (1981).
[41]M. Ben-Nun and T. J. Martínez, J. Phys. Chem. A **103**, 10517 (1999).
[42]W. H. Miller, J. Phys. Chem. A **105**, 2942 (2001).
[43]H. Wang and M. Thoss, Chem. Phys. **304**, 121 (2004).
[44]S. A. Egorov, E. Rabani, and B. J. Berne, J. Chem. Phys. **108**, 1407 (1998).
[45]J. G. Saven and J. L. Skinner, J. Chem. Phys. **99**, 4391 (1993).
[46]C. Spencer and R. F. Loring, J. Chem. Phys. **105**, 6596 (1996).
[47]A. Nitzan, *Chemical Dynamics in Condensed Phases* (Oxford University Press, 2006).
[48]S. Mukamel, J. Chem. Phys. **77**, 173 (1982).
[49]M. Wehrle, M. Šulc, and J. Vaníček, Chimia **65**, 334 (2011).
[50]M. Šulc, H. Hernández, T. J. Martínez, and J. Vaníček, J. Chem. Phys. **139**, 034112 (2013).
[51]L. Turi, H. Gyoergy, P. J. Rossky, and D. Borgis, J. Chem. Phys. **131**, 024119 (2009).
[52]O. Kühn and N. Makri, J. Phys. Chem. A **103**, 9487 (1999).
[53]G. Hanna and E. Geva, J. Phys. Chem. B **115**, 5191 (2011).
[54]Y.-C. Shen and J. A. Cina, J. Chem. Phys. **110**, 9793 (1999).
[55]R. Kapral and G. Ciccotti, J. Chem. Phys. **110**, 8919 (1999).
[56]C. C. Martens and J. Y. Fang, J. Chem. Phys. **106**, 4918 (1997).
[57]A. Donoso and C. C. Martens, J. Phys. Chem. A **102**, 4291 (1998).
[58]A. S. Petit and J. E. Subotnik, J. Chem. Phys. **141**, 014107 (2014).
[59]The evolution of the excited-state populations throughout the delay time essentially provides the initial conditions for the electronic coherence created by the probe pulse. This electronic coherence is then propagated exactly as in our previous study on linear absorption spectroscopy and therefore the semiclassical analysis presented there will hold here as well.
[60]J. C. Tully, J. Chem. Phys. **93**, 1061 (1990).
[61]J. C. Tully, Faraday Discuss. **110**, 407 (1998).
[62]Y. Tanimura and S. Mukamel, J. Chem. Phys. **101**, 3049 (1994).
[63]W. S. Sheu and P. J. Rossky, Chem. Phys. Lett. **213**, 233 (1993).
[64]U. Müller and G. Stock, J. Chem. Phys. **107**, 6230 (1997).
[65]A. Kelly and T. E. Markland, J. Chem. Phys. **139**, 014104 (2013).
[66]L. Wang and D. Beljonne, J. Chem. Phys. **139**, 064316 (2013).
[67]W. Xie, S. Bai, and Q. Shi, J. Phys. Chem. A **117**, 6196 (2013).
[68]M. Santer, U. Manthe, and G. Stock, J. Chem. Phys. **114**, 2001 (2001).
[69]J. E. Subotnik, W. Ouyang, and B. R. Landry, J. Chem. Phys. **139**, 214107 (2013).
[70]B. R. Landry, M. J. Falk, and J. E. Subotnik, J. Chem. Phys. **139**, 211101 (2013).
[71]B. R. Landry and J. E. Subotnik, J. Chem. Phys. **137**, 22A513 (2012).
[72]M. J. Bedard-Hearn, R. E. Larsen, and B. J. Schwartz, J. Chem. Phys. **123**, 234106 (2005).
[73]J.-Y. Fang and S. Hammes-Schiffer, J. Phys. Chem. A **103**, 9399 (1999).
[74]A. W. Jasper and D. G. Truhlar, J. Chem. Phys. **123**, 064103 (2005).
[75]F. Webster, E. T. Wang, P. J. Rossky, and R. A. Friesner, J. Chem. Phys. **100**, 4835 (1994).
[76]K. F. Wong and P. J. Rossky, J. Chem. Phys. **116**, 8418 (2002).
[77]J. E. Subotnik and N. Shenvi, J. Chem. Phys. **134**, 024105 (2011).
[78]E. Wigner, Phys. Rev. **40**, 749 (1932).
[79]W. B. Case, Am. J. Phys. **76**, 937 (2008).
[80]P. V. Parandekar and J. C. Tully, J. Chem. Phys. **122**, 094102 (2005).
[81]J. R. Schmidt, P. V. Parandekar, and J. C. Tully, J. Chem. Phys. **129**, 044104 (2008).
[82]W. Press, B. Flannery, S. Teukolsky, and W. Vetterling, *Numerical Recipes in FORTRAN 77: The Art of Scientific Computing*, Fortran Numerical Recipes Vol. 1 (Cambridge University Press, 1992).
[83]D. T. Colbert and W. H. Miller, J. Chem. Phys. **96**, 1982 (1992).
[84]G. A. Worth, H.-D. Meyer, and L. S. Cederbaum, in *Conical Intersections: Electronic Structure, Dynamics, and Spectroscopy*, edited by W. Domcke, D. R. Yarkony, and H. Köppel (World Scientific Publishing Co. Pte. Ltd., 2004), Chap. 14, pp. 619–698.
[85]See supplementary material at http://dx.doi.org/10.1063/1.4897258 for more extensive data sets comparing the method developed in this study to alternative semiclassical approaches for both the shifted harmonic potentials and three state models.

This article is copyrighted as indicated in the article. Reuse of AIP content is subject to the terms at: http://scitation.aip.org/termsconditions. Downloaded to IP: 74.109.53.69 On: Mon, 27 Oct 2014 11:47:44